Detection and Classification of Stroke Using Texture Analysis on CT Images

A Thesis submitted in the partial fulfillment of requirements for the award of the degree of

Master of Engineering

In

Electronic Instrumentation and Control Engineering

Submitted by

PRAMOD BHAT

Regn.No-801051012

Under the esteemed guidance of

Mr. M. D. Singh

Asst. Professor

Department of Electrical and Instrumentation Engineering

THAPAR UNIVERSITY

PATIALA (PUNJAB)-147004

June-2012

CERTIFICATE

I hereby declare that the Thesis entitled **Detection And Classification Of Stroke Images Using Texture Analysis on CT images** is an authentic record of my own work carried out as the requirements for the award of the degree of M.E. (Electronic Instrumentation and Control Engineering) at Thapar University, Patiala, under the guidance of **Mr.M.D Singh**, Assistant Professor, EIED.

The matter presented in this Thesis has not been submitted for the award of any other degree of this or any other university.

Pramod Bhat
(Roll no-801051012)

Date 20/6/2012

It is certified that the above statement made by the student is correct to the best of my knowledge and belief.

Mr.M.D Singh
Assistant Professor
Department of Electrical
and Instrumentation
Engineering

27/7/12
(Dilbag Singh)

Countersigned by:

S. Ghosh 25/6/12

Dr. Smarajit. Ghosh
Professor & Head,EIED
Thapar University, Patiala

Dr. S.K. Mohapatra
Dean, Academic Affairs
Thapar University, Patiala

ACKNOWLEDGEMENT

I would like to express my sincere gratitude to my supervisor, **Mr. M.D Singh,** Assistant Professor (EIED), for all his guidance and invaluable advises throughout the progress. He has stimulated my interest in medical image processing and inspired me for doing research on this topic.

I would also like to thank **Dr. Smarajit Ghosh**, Professor & Head, Electrical & Instrumentation Engg. Department, and **Dr. S.K Mohapatra**, Dean, Academic Affairs for giving an opportunity to work in this regard.

Dr. Virender Garg(MD) Sr. Resident, Department of Radiology, Govt. Rajindra hospital, Patiala, for extending all the needed help to carry out this work. Also I would like to thank my parents and all my friends for their continuous support and encouragement.

Pramod Bhat

ABSTRACT

Detection and diagnosis of various types of ailments and fractures is one of the fields that is highly dependent on medical image processing. The need for ccorrect diagnosis of the ailment type is very important for proper medication as any delay or wrong diagnosis may become fatal to the patient. Stroke is a disease that is caused by obstruction of the blood supply to the brain, or bleeding of blood into the brain. Any delay in administering right medicine may result in permanent disability or sudden death. Many methods have been developed to diagnose stroke using MRI images. In this work we have used Computed Tomography (CT) images for diagnosis stroke using texture features and classifiers. Five different classifiers are used and they are combined to get better diagnosis accuracy. The accuracy of classifier ensemble output is found to be 95% and the area under ROC (AUC) was found to be about greater than 0.95 for all the classes. The method proves very effective for diagnosis of stroke with good accuracy and able to differentiate acute, chronic and hemorrhage successfully.

TABLE OF CONTENTS

LIST OF ABBREVIATIONS

CT	*Computed Tomography*
MRI	*Magnetic resonance imaging*
ROC	*Receiver Operating Characteristics*
SPECT	*Single Photon Emission Computed Tomography*
PET	*Positron Emission Tomography*
ECG	*Electrocardiogram*
TIA	*Transient Ischemic Stroke*
TEM	*Law's Texture Energy Measures*
FDTA	*Fractal Dimension Texture Analysis*
SFM	*Statistical Feature Matrix*
FDR	*Fisher's Discrimination Ratio*
K-NN	*K-Nearest Neighbor Algorithm*
CART	*Classification using Regression*
SVM	*Support Vector Machine*
AUC	*Area Under The Curve*

LIST OF FIGURES

LIST OF TABLES

CHAPTER-1
INTRODUCTION

1.1 OVERVIEW

Image processing has long been used in diagnosis of various types of fractures and diseases in medical field. This particular field of image processing is called Medical Image processing. X-ray, Ultrasonic Imaging, Computed Tomography (CT), Magnetic Resonance Imaging (MRI) are some of such imaging techniques used. Each one of them has different sub-types as per the application and operating conditions. Computed Tomography is a variant of x-ray, but the scanning is taken from many angles in the former one and finally the 'slice' of the object is reconstructed using some techniques. Ultrasonic imaging uses very high frequency sound waves to scan the organ under test. MRI uses magnetic fields to make normal and abnormal tissues to behave differently so that its effect is differentially reflected in the reconstructed image. Some methods are preferred over other methods based on the part of the body to be scanned or some other technical and feasibility reasons. CT is preferred over MRI for scanning head in case of emergency as it takes very less time. Moreover CT imaging is less hazardous over MRI and gives better comfort.

Stroke is a physiological disorder caused either by bleeding inside brain or lack of blood supply to some part of the brain. It may result in disability, coma for many days or sudden death based upon the intensity of the stroke. Hence accurate diagnosis and proper medication is of prime importance in such cases. CT is one such method used for diagnosis of stroke that is preferred over many other techniques. For being having quick scanning ability and better comfort, it is a widely used scanning technique used all over the world. But the challenge with CT is that it does not properly highlight the abnormal area which makes the image difficult to accurately classify the disease or abnormality. This problem becomes more prominent when there is a slight difference between the normal and abnormal area. To tackle this, many variants of CT have been invented. But for such advanced variants being costly, many diagnostic laboratories, particularly in underdeveloped and developing countries, are not able to afford them. Hence finding a way to accurately classify the different types of stroke with already-existing technology would help physicians to accurately detect and medicate patients, and save many lives.

The objective of this thesis work is to detect and classify the stroke, if present. As already mentioned, the accurate classification of stroke type is of prime importance here. Texture analysis, which is a widely used medical analysis tool, is used in this work for extracting various features available in the image for further analysis. The unaffected portion of the brain is used as a reference basis. The texture features extracted from stroke affected region, also called as lesion, are then extracted for further processing. Because of the high dimension that is extracted from texture measurements, dimensionality reduction technique is used so that further processing and analysis becomes less complicated both in terms of calculation and analysis. Some of the best classifiers are then used for classification of the data extracted from the lesion. The final result shows that, the proposed algorithm has accuracy of nearly 95% and area under Receiver Operating Characteristics (ROC) near to 1 in many cases, which indicates that the method is highly reliable and accurate.

1.2 ORGANIZATION OF THESIS

This thesis is organized as given below.

The organization of the thesis work is as below. Chapter 1 includes the brief explanation of various kinds of medical imaging methods, a brief introduction to stroke and the objective of the work. Chapter 2 involves literature survey, which explains the various works that have been carried out in the area. Chapter 3 explains various kinds of stroke, their causes, diagnosis methods and precautions to prevent it. Various kinds of texture measurements, preprocessing of the data and classification techniques are explained in chapter 4. Chapter 5 presents results of analysis, and chapter 6 concludes the work with conclusion and future scope in this area.

CHAPTER-2
LITERATURE REVIEW

This chapter deals with various research works that were carried in past and contributed to this field of medical image processing. Even though the disease Stroke is as old as existence of living being on the planet earth, very little research work has been done in this regard. In early ages, people used to treat with some superstitious methods which still exist on various parts of earth. Since the advent of ultrasonic and CT scanning methods, the diagnosis and finding exact reason for this has become easy. Some of the related research works carried out in this regard is described below.

Chung *et.al* (1992) In this paper, the classification of ultrasonic liver images using texture analysis was presented. They used spatial gray-level dependence matrices, the Fourier power spectrum, the gray-level difference statistics, and the Laws' texture energy measures. Features of these types were used to classify three sets of ultrasonic liver images - normal liver, hepatoma, and cirrhosis (30 samples each). For getting better performance, a new texture feature set (called multi-resolution fractal features) based upon the concepts of multiple resolution imagery and fractional Brownian motion model was proposed to detect diffuse liver diseases fastly and accurately. A real time implementation of our algorithm was performed on a SUN 4/330 workstation and produces about 90% correct classification for the three sets of ultrasonic liver images.

Milan et.al (2001) presented a method for automated segmentation of stroke lesion. The method consists of three steps. The first step is automated determination of axial symmetry of head. In the second step The first step is automatic In the second step the seeded region-growing (SRG) algorithm is used to segment input image into number of regions having uniform brightness. Features of these regions, such as brightness, area, neighbourhood and relative position to symmetry axis are used to create facts for a rule-based expert system. Based on created facts and pre-defined rules as input, the rule-based expert system is used in the third step to label regions as background, scull, gray/white matter, CSF and stroke. Experimental results have been conducted and have demonstrated the feasibility and accuracy of the proposed method.

Vidya Manian *et.al*.(2000) proposed a new algorithm for texture classification based on logical operators is presented. Operators constructed from logical building blocks were

convolved with texture images. An optimal set of six operators were selected based on their texture discrimination ability. The responses were then converted to standard deviation matrices computed over a sliding window. Zonal sampling features were computed from these matrices. A feature selection process was applied and the new set of features was used for texture classification. Classification of several natural and synthetic texture images were presented demonstrating the excellent performance of the logical operator method. The computational superiority and classification accuracy of the algorithm is demonstrated by comparison with other popular methods. Experiments with different classifiers and feature normalization are also presented. The Euclidean distance classifier is found to perform best with this algorithm. The algorithm involves only convolutions and simple arithmetic in the various stages which allows faster implementations. The algorithm is applicable to different types of classification problems which are demonstrated by segmentation of remote sensing images, compressed and reconstructed images and industrial images.

Christodoulou *et.al*. (2003) proposed a work on morphology based analysis, using texture analysis, of carotid plaque using high resolution ultrasound images. The objective of the study was to develop a computer-aided system that would facilitate the characterization based on texture analysis of the carotid plaque for the identification of individuals with asymptomatic carotid stenosis at risk of stroke. A total of 230 plaque images were collected which were classified into two types: symptomatic because of ipsilateral hemispheric symptoms, or asymptomatic because they were not connected with ipsilateral hemispheric events. Ten different texture feature sets were extracted from the manually segmented plaque images using the following algorithms: first-order statistics, spatial gray level dependence matrices, gray level difference statistics, neighbourhood gray tone difference matrix, statistical feature matrix, Laws texture energy measures, fractal dimension texture analysis, Fourier power spectrum and shape parameters. For the classification task a modular neural network composed of self-organizing map (SOM) classifiers, and combining techniques based on a confidence measure were used. Combining the classification results of the ten SOM classifiers inputted with the ten feature sets improved the classification rate of the individual classifiers, reaching an average diagnostic yield (DY) of 73.1%. The same modular system was implemented using the statistical k-nearest neighbour (KNN) classifier. The combined DY for the KNN system was 68.8%. The results of this paper show that it is possible to identify a group of patients at risk of stroke based on texture features extracted from ultrasound images of

carotid plaques. This group of patients may benefit from a carotid endarterectomy whereas other patients may be spared from an unnecessary operation.

Andrius *et.al.(*2004) described a new method to segment ischemic stroke region on computed tomography (CT) images by utilizing joint features from mean, standard deviation, histogram, and gray level co-occurrence matrix methods. For better recognition 31×31 sliding window was used. The method differentiated only two areas-stroke and not-stroke. Thresholding technique was used for this. The presented unsupervised segmentation technique shows ability to segment ischemic stroke region with less fault region.

Ashok Srinivasam *et.al.(*2006) described many aspects of CT and MRI imaging. They delineated types of CT and MRI scans and their merits and demerits and order of preference.. The compared various properties of CT and MRI related to emergency monitoring of patients.

Fei Peng *et.al* (2008) proposed an effective pre-processing method for CT brain images to provide consistent feature foe content based image retrieval . The key steps include correcting lean of the imaging angle, cutting off background region ,and normalization. Vast numbers of images of the same patient at different anatomical angles were taken and the result was verified. Finally the enhanced images were contrast overlapped to test the effectiveness of the method. It was verified that the method was very effective and accurate.

Elzbieta and Grzegorz (2008) proposed an easy way of finding stroke on CT images. By calculating a cohesive rate of suspicious pixels on a series of CT images there is a probability of calculating a general probability of a stroke. The method provided also tuning capabilities like Sensitivity factor and precision parameter for finding different types of strokes. The method also provided an option for displayable graph for additional analysis of brain. The experiment was carried out on many patients and the method was found successful in detecting many types of stroke.

Mayak Chawla *et.al.* (2009) devised a new method to classify an abnormal CT image into acute, haemorrhage and chronic infarct. The method consists of three steps: Image enhancement, detection of midline symmetry and analysis. Two level classifications was used to detect abnormality using intensity based and wavelet transforms. The method gives 90% accuracy and 100% recall in detecting abnormality at patient level. It achieved an average precision of 91% at the slice level. The key feature of this method was it's

ability to detect and segment all types of stroke. But one exceptional case where stroke occurs symmetrically on both sides of symmetry line was not discussed in this method.

Rajendran *et.al.* (2010) proposed a system that mainly concentrates on the diagnosis of brain tumour from the CT images of brain. The work gives the neuro-radiologist a second opinion for the easy identification of tumour cells from the brain image. The important data mining concept that has been included in the work consists of pre-processing of the CT scan brain image. The method used for pre-processing includes Shape priori technique. The feature selection from the brain image was done using the association rule mining. The rules generated for extracted features are stored in the transactional database have been classified using the data mining concept called Decision Tree Classification. The combination of both the association rule mining and the decision tree classification gives the high degree of accuracy and efficiency for the proposed system.

Kakkos *et.al*.(2011) discussed a method to use texture measurements to classify carotid plaque and its correlation of possibility of occurrence of ischemic stroke. They measured many texture features from Fourier Power Spectrum (FPS), Gray Level Difference Statistics (GLDS), Spatial Gray Level Dependence Matrices (SGLDM) for analysis of carotid plaque on ultrasonic images. Using the method they could achieve accuracy of 86 % and area of 0.92 under ROC. Hence they proved that texture analysis of carotid plaque could be best ways to predict possibility of stroke.

Fueanggan *et.al.* (2011) proposed a method to predict ischemic stroke area from ct perfusion images of cbv and cbf based on digital image processing techniques. The objective of the research was to specify Ischemic Stroke Area by assigning Threshold level of Computed Tomography Perfusion (CTP) from CBV (Cerebral Blood Volume) and CBF (Cerebral Blood Flow) images. By matching some of the key identities extracted, they separated the brain into left and right to specify Ischemic Stroke Area. As a result of experiment in 10 Stroke patients sample by setting CBV Threshold level to 2.5 ml/tOOg (±l.S) and CBF Threshold level to 20 ml1100g/min (±to), the distribution of key identities depends on their threshold. So they could sort elementary information of left and right side of the brain to specify Ischemic Stroke Area in order to compare the results with brain specialists.

CHAPTER-3
STROKE

3.1 INTRODUCTION TO STROKE

In general stroke can be defined as a condition where clot of blood in the blood vessels carrying blood to brain leads to scarcity of blood supply to the brain or leakage of blood into the brain which results in death of brain cells which eventually results in disability. World Health Organization defines it as “"neurological deficit of cerebrovascular cause that persists beyond 24 hours or is interrupted by death within 24 hours".

Stroke is one of the largest cause of death and third largest cause of death in U.S. According to a study carried out, approximately 20 million people suffer from stroke every year and 5 million of them die. And stroke is the major risk factor for those who aged above 65. Even though death certificates are not well documented in India, it was estimated by World Health Organization that 0.63 million deaths are caused by stroke only in India. Some of the astonishing facts about stroke morbidity and mortality are listed out below.

- Prevalence 55.6 per 1000,000 all ages.
- 0.63 Million deaths (World Health Organization survey 2005[1]).
- 1.44-1.64 million cases of new acute strokes every year (World Health Organization survey 2005[2])
- 6,398,000 DALYs (World Health Organization survey 2009[2])
- 12% of strokes occur in the population aged <40 years [3]
- 28-3- case fatality ranges from 18-41% (Dalal et.al. 2008 [2])

From a study carried out it was found that urban population is more prone to stroke compared with rural population. Because of western life style and less physical work, nowadays it has made its presence in rural areas also remarkably. An international study showed that developing countries are showing increased number in stroke cases than developed countries.

As life expectancy is expected to increase in India, number of stroke patients is also expected increase. It is showed that three transitions have major contribution to stroke epidemic in India. They are demographic, socioeconomic and lifestyle. Lifestyle and socio economic conditions have raised the risk factor in rural areas. But these are modifiable. Non modifiable factors include heredity, age, low birth weight etc.

3.2 CAUSES OF STROKE

There are two types of strokes,

1. Ischemic stroke, which is categorized in to
    a) Acute
    b) Chronic
2. Haemorrhage stroke.

Ischemic stroke is the case when blood clots in the vessels leading to the brain. When blood flow is stopped for more than a few seconds, the brain cells do not get sufficient oxygen and they start dyeing. This particular phase is called Acute stroke. In this situation the cells have not started decaying yet. After couple of hours or days of occurrence of clot, the cells start decaying rapidly and become completely dysfunctional. This phase is called Chronic stroke.

Haemorrhage is caused when blood vessels ruptures inside brain which results in leakage of blood into the brain. Due to high blood pressure hence created brain gets damaged. The figures 3.1, 3.2 and 3.3 shows Acute, Chronic and Haemorrhage stroke affected CT images respectively.

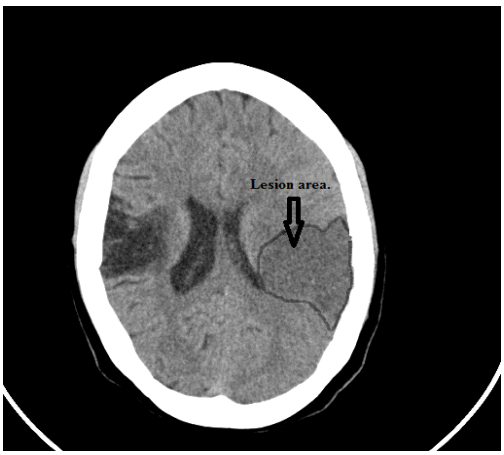

Fig 3.1 Image showing Acute lesion area.

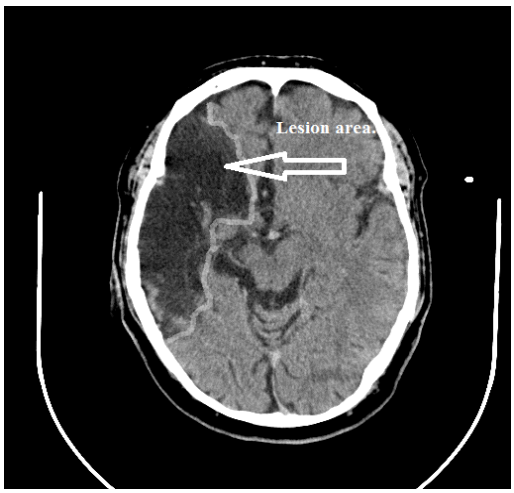

Fig 3.2 Figure showing Chronic lesion area

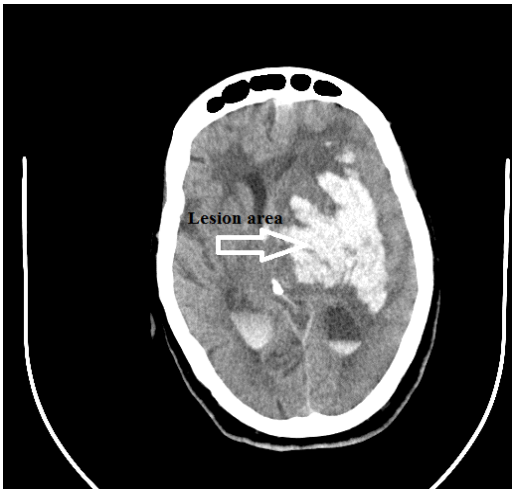

Fig 3.3 Figure showing Hemorrhage lesion

3.3 SYMPTOMS OF STROKE

When brain cells are deprived of oxygen their normal functionalities are altered. The extent of damage on the patient depends on the area of brain that has been affected and amount of tissue damage. Some of the general and early symptoms are listed below.

1. Sudden numbness or weakness of the face, arm or leg, especially on one side of the body.
2. The loss of voluntary movement and/or sensation may be complete or partial. There may an associated tingling sensation in the affected area.
3. Sudden confusion or trouble speaking or understanding. Sometimes weakness in the muscles of the face can cause drooling.
4. Sudden trouble seeing in one or both eyes
5. Sudden trouble walking, dizziness, loss of balance or coordination
6. Sudden, severe headache with no known cause

3.4 DIAGNOSIS OF STROKE

When a patient shows aforementioned symptoms the physician should not jump to conclude the patient as stroke affected. There are some other reasons which can show similar symptoms. They are,

1. brain tumours,
2. brain abscess (a collection of pus in the brain caused by bacteria or a fungus),
3. migraine headache,
4. bleeding in the brain either spontaneously or from trauma,
5. meningitis or encephalitis,
6. an overdose of certain medications, or
7. an electrolyte imbalance in the body. Abnormal concentrations (too high or too low) of sodium, calcium, or glucose in the body may also cause changes in the nervous system that can mimic a stroke.

Many modern methods are available, such as CT [4] and MRI [5] along with other methods [6], for better understanding of certainty of stroke. They are explained in this section.

3.4.1 CT Imaging.

CT scanning is the most widely used imaging method to evaluation of stroke under emergency conditions. CT scan is quick and comfortable. But in some cases, particularly if the stroke is in initial stages, a CT image may not yield good diagnostic information. . This may be because of very small area affected or the machine may not be able to scan a particular area of brain. But still this is the first diagnostic tool that comes into physicians mind when he/she wants a patient to check for a possible stroke.

3.4.1.1 Working of CT

CT machine uses normal x-rays to scan a particular part of a body. But unlike normal x-ray which are used to assess the damage to bones, a rotating sensor-source set in the CT machine takes the scan at different angles and finally it re-constructs a ‘slice’ of the part

scanned[7]. The figure 3.5 shows a typical CT machine. The figure 3.6 shows a conceptual diagram of a CT machine.

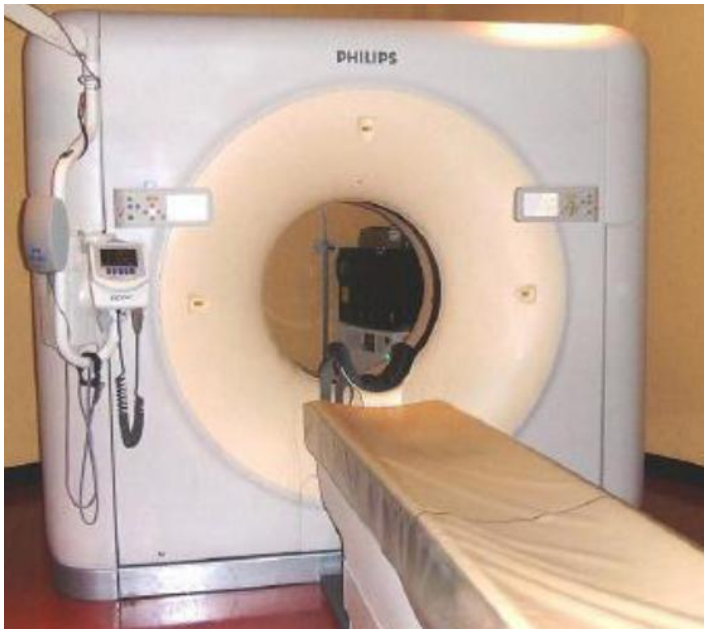

Fig 3.4 A typical CT machine.

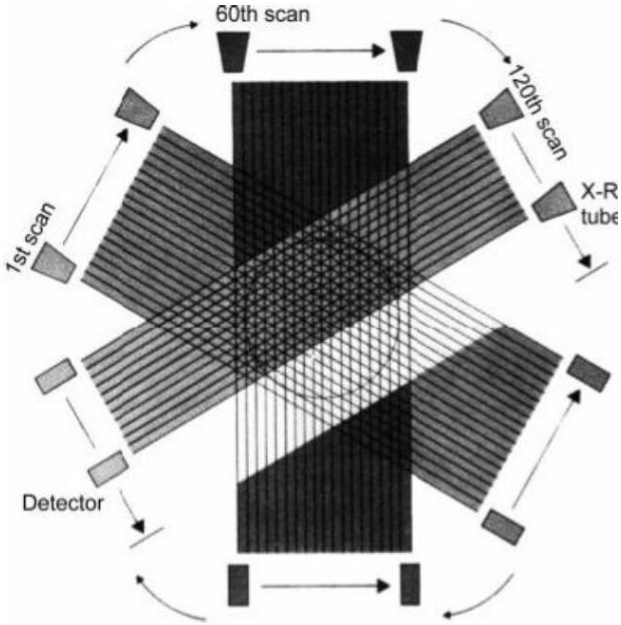

Fig 3.5 Conceptual diagram showing how scan is done.

3.4.2 SPECT scan.

A *single photon emission computed tomography* (SPECT) scan captures images of the brain using both an imaging camera and an injection of a radioactive material into the body. SPECT imaging shows blood flow to the brain and can provide information early in the course of a stroke, before changes show up on a CT scan or MRI. The drawback of this test is that it can't distinguish between ischemic and hemorrhagic strokes.

3.4.3 PET scan.

A *positron emission tomography* (PET) scan uses radioactive material that is injected into the body to pinpoint areas of the brain with the greatest chemical activity. After the radioactive material is injected, the scanning machine reads how much energy is emitted from the brain, and creates a picture of the brain from that reading. PET is helpful in determining the extent of damage to the brain.

3.4.4 MRI Scan.

MRI (magnetic resonance imaging) uses a large magnetic field to produce an image of the brain. Like the CT scan, it shows the location and extent of brain injury. The image produced by MRI is sharper and more detailed than a CT scan, so it's often used to diagnose small, deep injuries.

Conventional spin-echo MRI is more sensitive and more specific than CT for the detection of acute cerebral ischemia within the first few hours after the onset of stroke. It has the additional benefit of depicting the pathologic entity (stroke and its mimics) in multiple planes. The MR sequences typically used in the evaluation of acute stroke include T1-weighted spin-echo, T2- weighted fast spin-echo, fluid-attenuated inversion recovery, T2*-weighted gradient-echo, and gadolinium-enhanced T1-weighted spin-echo sequences. Typical MRI findings in patients with hyperacute cerebral ischemia include hyperintense signal in white matter on T2- weighted images and fluid-attenuated inversion recovery images, with a resultant loss of gray matter– white matter differentiation analogous to the loss at CT; sulcal effacement and mass effect; loss of the arterial flow voids seen on T2- weighted images; and stasis of contrast material within vessels in the affected territories. The table 3.1 compares MRI with CT. Table 3.2 compares sensitivity and specificity of MRI and CT

Table 3.1 Comparison of CT and MRI for Evaluation of Acute Stroke

Characteristic	**CT**	**MRI**
Availability	Good	Fair
Examination Time	5	20
Imaging volume for perfusion study	2-4 cm	Entire brain
Radiation	Ionizing radiation associated with potential risks for cancer	No ionizing radiation
Contrast material	Iodinated contrast medium is mandatory, and patients incur higher risks for anaphylaxis and toxic effects on the kidneys	Gadolinium-based contrast medium is mandatory, with a minimally increased risk for toxic effects on the kidneys

Table 3.2 The comparison of sensitivity and specificity of CT and MRI

Parameter	**CT scan**	**MRI scan**
For diagnosing ischemic stroke in the emergency setting		
Sensitivity	**16%**	**83%**
Specificity	**96%**	**98%**
For diagnosing hemorrhagic stroke in the emergency setting		
Sensitivity	**89%**	**81%**
Specificity	**100%**	**100%**

3.4.5 Stroke Diagnosis: Some Other Tests.

Seeing the condition of key blood vessels and of the heart gives doctors other important pieces of information when someone has a stroke.

- **Ultrasound.** An ultrasound test can be performed on the carotid arteries in the neck, the blood vessels that supply blood to the brain. Images are taken using an ultrasound device that emits sound waves at very high frequencies. These images reveal how well, or how poorly, blood is flowing through the carotid arteries. A narrowed or blocked carotid artery can lead to a stroke.

- **Cerebral angiogram.** Sometimes called cerebral angiography or arteriogram, this imaging test uses a special dye and X-rays to view the blood vessels supplying the brain. A cerebral angiogram can show narrowed or blocked arteries, as well as other abnormalities that can potentially cause a stroke, such as an aneurysm, which is a dilated blood vessel, or an AVM, which stands for arteriovenous malformation, a knotted group of arteries and veins that are prone to bleeding. This test can diagnose both ischemic and hemorrhagic strokes, but is usually not a first-line test.

- **Electrocardiogram (ECG).** An ECG gives information on the electrical activity of the heart, including heart rate and rhythm. Electrodes are placed on the body and record the heart's electrical activity. An irregular heart rhythm such as atrial fibrillation can lead to blood clots within the heart that could travel to the brain and cause a stroke. Every patient suspected of having a stroke will have an ECG.

- **Echocardiogram.** This test uses ultrasound waves to make an image of the heart. It can detect the presence of a clot within the heart that could lead to stroke.

3.5 PREVENTION OF STROKE

The possibility of suffering a stroke can be reduced by controlling the risk factors [8]. Some of the major risk factors are explained below here.

Controlling Blood Pressure: High blood pressure is the main risk factor of stroke. The chances of getting stroke are increased by the amount of the blood pressure above the normal range. Keeping it under control can help get rid of stroke.

Avoid Smoking: An important stroke risk factor is cigarette smoking or tobacco use. Chemicals in tobaccos are associated with developing atherosclerosis or narrowing of the arteries in the body. This narrowing can involve the large carotid arteries as well as

smaller arteries within the brain. Smoking is also a major risk factor in heart disease and artery disease. Use of tobacco can also make heart weak which leads to insufficient blood supply to the brain.

Controlling Diabetes: Increased level of sugar in blood can block small blood vessels permanently. In case if it happens in brain it will result in deficiency of blood to some parts of the brain.

Limiting Cholesterol Level: High cholesterol in blood eventually results in blockage of blood vessels. Keeping it under control by good diet can decrease risk factor of stroke.

Blood Thinners: Irregular heart beat called arterial fibrillation can cause blood clots in the upper chambers of the heart. When these clots move to brain along with blood it results in blockage of blood flow in smaller veins which eventually results in stroke. Blood thinners like Warfarin and Aspirin can prevent clot of blood when administrated to the body in proper quantities. Also if a person is having stroke history taking blood thinners like Aspirin can prevent stroke from happening second time.

Antiplatelet therapy: Many TIA (Transient Ischemic Stroke) and stroke patients may benefit from antiplatelet drugs which reduces the tendency of blood to clot. Adverse effects may include increased bleeding in case of injuries.

Carotid Endarterectomy: In many cases, a person may suffer a TIA or a stroke that is caused by the narrowing or of the carotid arteries (the major arteries in the neck that supply blood to the brain). If left untreated, patients with these conditions have a higher risk of experiencing a major stroke in the future. An operation that cleans out the carotid artery and restores normal blood flow is known as a carotid endarterectomy. This procedure has been shown to markedly reduce the incidence of a subsequent stroke. In patients who have a narrowed carotid artery, but no symptoms, this operation may be indicated in order to prevent the occurrence of a first stroke.

From the above discussions, we can conclude that CT imaging is the best way to diagnose the stroke, considering both time taken and hazard caused to the patient compared to MRI. The stroke once affected is almost incurable, but can be prevented by taking proper diet and avoiding smoking, junk foods etc.

CHAPTER-4
MATERIALS AND METHODOLOGY

4.1 TEXTURE ANALYSIS

4.1.1 INTRODUCTION

Many real objects in nature do not possess uniformity in their surface structure or the way they reflect light. Instead they show some repetitive pattern. In broad this repetitive pattern can be defined as texture. In other way texture can be understood as uniformity in being non-uniform. But there is no clear definition of texture. Many pioneers in different fields have defined the word texture in different ways applicable to their field and work. Some of the definitions which can give broad understanding of texture are given below.

- "We may regard texture as what constitutes a macroscopic region. Its structure is simply attributed to the repetitive patterns in which elements or primitives are arranged according to a placement rule." [9]
- "A region in an image has a constant texture if a set of local statistics or other local properties of the picture function are constant, slowly varying, or approximately periodic."[10]
- "The notion of texture appears to depend upon three ingredients: (i) some local 'order' is repeated over a region which is large in comparison to the order's size, (ii) the order consists in the non-random arrangement of elementary parts, and (iii) the parts are roughly uniform entities having approximately the same dimensions everywhere within the textured region."

For a layman eye is a god gifted instrument which sees everything at a glance. But in-fact our visual system does not 'sees' a scene; it tries to understand and compare different objects in the 'scene'. The process of seeing a scene is so much complicated that only a person working on brain or machine vision can understand the complexity and process behind it. Normally when we see a scene we just look at the global variations in it. We do not really look at the local variations and the reason behind why different scenes and objects really look different i.e. texture. Figure 4.1 shows some of the natural and synthetic texture pictures which can help us understand the meaning of texture and importance of local and global patterns which actually differentiate different objects in a scene. The next section explains various texture features and meanings of them.

Fig 4.1 Figure showing various natural and a synthetic texture based images.

4.1.2 FEATURE EXTRACTION TECHNIQUES

Consider a two dimensional image *f(x,y)* where *x=0,1,.....N-1 and y=0,1,....M-1*. The function *f(x,y)* can take *G* discrete intensity levels ranging from 0 to *G*-1.Then the intensity-level histogram is a function showing (for each intensity level) the number of pixels in the whole image, which have this intensity:

$$h(i)= \sum_{x=0}^{N-1} \sum_{y=0}^{M-1} (\delta(f(x,y),i) \qquad (4.1)$$

Where δ(j,i) is the Kronecker delta function [11].

$$\delta(j,i)=\begin{cases}1, & j=i\\ 0, & j\neq i\end{cases} \qquad (4.2)$$

Dividing the values of h(i) by total number of pixels gives probability density of occurrence of the intensity levels. Mathematically it can be expressed as,

$$p(i)=h(i)/NM,\ i=0,1,.....G-1 \qquad (4.3)$$

4.1.3 FIRST ORDER STATISTICS

Since calculation of histogram involves single pixels the histogram contains first-order statistical information of that image [12]. We can derive many first-order texture expressions using the aforementioned equations .

Mean: $\mu=\sum_{i=o}^{G-1} ip(i)$ (4.4)

Variance: $\sigma^2=\sum_{i=o}^{G-1}(i-\mu)^2$ (4.5)

Skewness: $\mu_3=\sigma^{-3}\sum_{i=o}^{G-1}(i-\sigma)^3 p(i)$ (4.6)

Kurtosis: $\mu_4=\sigma^{-4}\sum_{i=o}^{G-1}(i-\mu)^4 p(i)-3$ (4.7)

Energy: $E=\sum_{i=o}^{G-1}[p(i)]^2$ (4.8)

Entropy: $H=-\sum_{i=o}^{G-1} p(i)^2 log_2[p(i)]$ (4.9)

The mean takes the average level of intensity of the image or texture being examined, whereas the variance describes the variation of intensity around the mean. The skewness is zero if the histogram is symmetrical about the mean, and is otherwise either positive or negative depending whether it has been skewed above or below the mean. Thus μ_3 is an indication of symmetry. The kurtosis is a measure of flatness of the histogram.

4.1.4 LAW'S TEXTURE ENERGY MEASURES (TEM)

Laws Texture energy measures [13] are derived from three vectors of length 3: *L3=(1,2,1),E3=(-1,0,1*), and *S3=(-1,2,1).* These three vectors represent one-dimensional operations of centre-weighted local averaging, symmetric first differencing for edge detection, and second differencing for spot detection respectively. If these vectors are convolved with themselves, we obtain new vectors of length 5. They are *L5=(1,4,6,4,1),E5=(-1,-2,0,2,1), and S5=(-1,0,2,0,-1).* By further self-convolution, we get new vectors of length 7. They are *L7=(1,6,15,20,15,6,1),E7=(-1,-4,-5,0,5,4,1),* and *S7=(-1,-2,1,4,,1,-2,-1),* where L7 performs local averaging, E7 acts as a edge detector, and S7

acts as a spot detector. If the column vectors of length l are row vectors of the same length, we obtain law's $l \times l$ masks. Following combinations can be obtained.

$LL = L7^t * L7$

$LE = L7^t * E7$

$LS = L7^t * S7$

$EL = E7^t * E7$

$EE = E7^t * E7$

$ES = E7^t * S7$

$SL = S7^t * L7$

$SE = S7^t * E7$

$SS = S7^t * S7$

To extract texture features from an image, these masks are convolved with the image, and statistics of this image are used to describe texture. The following texture features are extracted.

LL : texture energy from *LL* kernel

EE: texture energy from *EE* kernel

SS: texture energy from *SS* kernel

LE : average texture energy from *LE* and *EL* kernels

$LE = (LE + EL)/2$

ES: average energy from *ES* and *SE* kernels

$ES = (ES + SE)/2$

LS: average energy from *LS* and *SL* kernels.

$LS = (LS + SL)/2$

For feature extraction, following nomenclatures are used.

Technical Name	Nomenclature Used
LL	TEM1
EE	TEN2
SS	TEM3
LE	TEM4
ES	TEM5
LS	TEM6

4.1.5 FOURIER POWER SPECTRUM

The discrete Fourier transform of N×N point(pixels in our case) is given by

$$F(u,v) = \sum_{i,j=0}^{n-1} f(i,j)\, e^{-3\Pi} \sqrt{-1(iu,jv)} \quad (4.10)$$

where $0 \leq u$ and $v \leq N-1$.

The sample Fourier spectrum is defined by

$$\Phi(u,v) \equiv F(u,v)\, F^*(u,v) = |F(u,v)|^2 \quad (4.11)$$

where Φ is the sample power spectrum, and * denotes the complex conjugate. Coarse texture will have values of $|F|^2$ concentrated near the origin, whereas in fine texture, the values will be more spread out. The standard set of texture features used are ring-and wedge shaped samples of FPS [14].

Radial Sum:

Radial sum is defined as

$$\Phi_{r1,r2} \equiv \sum_{r1*r1 \leq u*u < r2*r2} |F(u,v)|^2 \quad (4.12)$$

Angular Sum:

Angular sum is defined as

$$\Phi_{\theta 1,\theta 2,} \equiv \sum_{\theta \leq (1/tan\left(\frac{v}{u}\right)) \leq \theta 2} |F(u,v)|^2 \quad (4.13)$$

for various angles θ_1 and θ_2.

4.1.6 FRACTAL DIMENSION TEXTURE ANALYSIS (FDTA)

Fractal dimension texture features [15] are used to describe the roughness of natural surfaces. It considers naturally occurring surfaces as the end result of random walks. Fractals provide a succinct and accurate method for describing natural objects that would previously have been described by spheres, cylinders and cubes. However, these descriptors are smooth, which makes modelling irregular natural scenes, or surfaces, very difficult. The fractal dimension describes the degree of irregularity or texture of a surface. With this approach rougher, or more irregular, structures have a greater fractal dimension. An important parameter to represent a fractal dimension is the fractal dimension D_f. Theoretically it can be estimated by the equation,

$$MF \equiv (H^{m,} H^{m-1}, \ldots\ldots H^{m-n+1}) \quad (4.14)$$

A simpler method is to estimate the H parameter from the equation,

$$E(|\Delta I|) = k(\Delta r)^H. \quad (4.15)$$

Where $E(\ )$ denotes the expectation parameter, , c is a constant, and Δr is the distance between two pixels, ΔI is the intensity difference between two pixels and,

$$k = E(|\Delta I|)_{\Delta r=1}. \quad (4.16)$$

By applying the log function we obtain

$$\log E(|\Delta I|) = \log k + H \log(\Delta r) \quad (4.17)$$

from Equation 3.17, the H parameter can be estimated , and the fractal dimension D_f can be computed from the relationship

$$D_f = 3 - H \quad (4.18)$$

A smooth surface is described by a small value of the fractal dimension D_f, and a the reverse applies for a rough surface.

Given an M×M image, the intensity difference vector is defined as

$$IDV \equiv [id(1), id(2), \ldots\ldots id(s)] \quad (4.19)$$

where s is the maximum possible scale, and $id(k)$ is the average of the absolute intensity difference of all the pixel pairs with vertical or horizontal distance k. The value of the parameter H can be obtained by using least squares linear regression to estimate the slope of the curve of $id(k)$ vs. k in log-log scales.

If the image is seen under different resolutions, then the multi-resolution (MF) fractal feature vector is defined as

$$MF \equiv (H^{m}, H^{m-1}, \ldots\ldots H^{m-n+1}) \quad (4.20)$$

where $M=2^m$ is the size of the original image, H^k is the H parameter estimated from image I^k, and n is the number of resolutions chosen. The multi-resolution fractal feature vector describes also the lacunarity of the image. It can be used for separation of textures with the same fractal dimension Df by considering all but the first components of the MF vectors.

4.1.7 STATISTICAL FEATURE MATRIX (SFM)

The statistical-feature matrix measures [16] the statistical properties of pixel pairs at several distances. Suppose $I(x,y)$ be the intensity at (x,y), and let $\delta=(\Delta x,\Delta y)$ represent the intersample-spacing distance vector, where Δx and Δy are integers. The δ contrast, δ covariance and δ dissimilarity are defined as

$$CON(\delta) \equiv E\{[I(x,y)-I(x+\Delta x,y+\Delta y)]^2\} \quad (4.21)$$

$$CON(\delta) \equiv E\{[I(x,y)-\eta] * [I(x+\Delta x, y+\Delta y)-\eta]\} \quad (4.22)$$

$$DSS(\delta) \equiv E\{[I(x,y)-I(x+\Delta x,y+\Delta y)]\} \quad (4,23)$$

where $E\{\}$ denotes the expextation operation and η is the average gray level of the image.

A statistical-feature matrix(SFN), M_{sf}, is an $(Lt+1)\times(2Lc+1)$ matrix whose (i,j) element is the d statistical feature of the image, where $d=(j-Lc,i)$ is an intersample spacing distance vector for $i=0,1,\ldots.Lt$, $j=0,1,\ldots\ldots Lc$, and where Lt,Lc are the constants that determine the

maximum intersample spacing distance. In a similar way, the contrast matrix*(M_{con})*, and dissimilarity matrix *(M_{dss})* can be defined as the matrices whose *(i,j)* elements are the *d* contrast, *d* covariance and d dissimilarity, respectively. Based on SFM the texture features-coarseness, contrast, periodicity and roughness, can be computed.

Coarseness:

Coarseness is defined as

$$F_{CRC}=C/\sum_{(i,j)\epsilon Ne}\frac{DSS(i.j)}{n} \quad (4.24)$$

where *c* is the normalizing factor, N_r is the set of displacement vectors defined as $N_r=\{(I,j):|\ i|,\ |j|\leq r\}$ and *n* is the number of elements in the set. A pattern is coarser than another when the two differ only in scale, with the magnified one being the coarser and having a larger F_{CRS} value.

Roughness :

It is expressed as

$$F_{RGH}=(D_f^{(u)}+ D_f^{(v)}/2 \quad (4.25)$$

where D_f is the fractal dimension in vertical and horizontal directions. D_f =3-*H*, and $E\{|\Delta I|\}=k(\delta)^H$, where H is estimated from the dissimilarity matrix. Larger the *Df*, rougher is the image.

Periodicity

It is defined as

$$F_{PER}= (\bar{M}_{dis}-M_{dis}(valley))/M_{dis} \quad (4.26)$$

where $\bar{M}_{dis}$ is the mean of all elements in M_{dss}, and $M_{dss}(valley)$ is the deepest valley in the matrix. Periodicity measures the appearance of periodicity repeated patterns in the image.

Contrast:

Contrast id defined as

$$F_{CON}=[\sum_{(i,j)\epsilon Nr} CON(i,j)/4]^{1/2} \quad (4.27)$$

It defines degree of sharpness of the edges in the image.

4.1.8 CO-OCCURRENCE MATRIX BASED TEXTURE FEATURES

One of the major statistical methods used in texture analysis is the one based on joint probability distributions of pairs of pixels.

The second order histogram is defined as the co-occurrence matrix [17] $h_{d,(I,j)}$. When this matrix is divided by total number of neighboring pixels $R(d,\theta)$ in the image, this matrix gives the estimate of joint probability $Pd_{\theta}(I,j)$ of two pixels, where d is the distance between two pixels at a given direction θ having particular values i and j. Consider two pixels (k,l) and (m,n). Suppose these pixels have gray level i *and* j. The estimated probability-density function will be donated by $P(I,j,d,\theta)$. consider an N×M image, let $Lx\{1,2,...Nx\}$ be the horizontal spatial domain, $Ly=\{1,2,.....Mx\}$ be the vertical spatial domain, and $I(x,y)$ be the image intensity at pixel (x,y). Consider the quantization level of angles be 45^0 intervals. Following texture measures can be extracted from the spatial grey-level-dependence matrices.

Angular Second Moment

It is the measure of homogeneity of the image.

$$f_1=\sum_i \sum_j \{p(i,j)\}^2 \quad (4.28)$$

Contrast

Contrast is the measure of the amount of local variations present in the image.It is defined as

$$f_2=\sum_{i=1}^{N-1} n^2 \sum_i \sum_j \{p(i,j)\} \quad (4.29)$$

Correlation

Correlation is a measure of gray-tone dependencies.

$$f_3=(\sum_i \sum_j (i,j)p(i,j) - \mu_{x^*}\mu_y/(\sigma_{x^*}\sigma_y) \quad (4.30)$$

where μ_x,μ_y and $\sigma_x\,\sigma_y$ are the mean and standard deviation values of p_x,p_y.

Variance

$f_4=\sum_i \sum_j (i-\mu)^2 p(i,j)$ (4.31)

Inverse Difference Moment

$f_5=\sum_i \sum_j p(i,j)^2/(1+(i-j)^2$ (4.32)

Sum Average

$f_6=\sum_{i=2}^{2Nx} ip_{x+y}(i)$ (4.33)

Sum Variance

$f_7=\sum_{i=2}^{2Nx}(i-f6)p_{x+y}(i)$ (4.34)

Sum Entropy

$f_{8=}\sum_{i=2}^{2Nx} p_{x+y}(i)\ log\ \{p_{x+y}(i)\}$ (4.35)

Entropy

$f9=\sum_i \sum_j p(i,j)\ log\big(p(i,j)\big)$ (4.36)

Texture features used in our study have been explained in Sections 4.1.2 to 4.1.8. In a total 29 texture measures have are explained out of which 26 features are used. These are summarized in a table below.

Table 4.1 Summary of all the texture measures.

Texture Measure	**Mathematical Expression.**
First Order Statistics	
Mean	$\mu=\sum_{i=o}^{G-1} ip(i)$
Variance	$\sigma^2=\sum_{i=o}^{G-1}(i-\mu)^2$
Skewness	$\mu 3=\sigma^{-3}\sum_{i=o}^{G-1}(i-\sigma)^3 p(i)$
Kurtosis	$\mu_4=\sigma^{-4}\sum_{i=o}^{G-1}(i-\mu)^4 p(i)$ -3
Energy	$E=\sum_{i=o}^{G-1}[p(i)]^2$
Entropy	$H=-\sum_{i=o}^{G-1} p(i)^2 log_2[p(i)]$
Law's Texture Energy Measures	
TEM1	texture energy from *LL* kernel
TEM2	texture energy from *EE* kernel

TEM3	texture energy from *SS* kernel
TEM4	$LE=(LE+EL)/2$
TEM5	$ES=(ES+SE)/2$
TEM6	$LS= (LS+SL)/2$
Fourier Power Spectrum	
Radial Sum	$\Phi_{r1,r2} \equiv \sum_{r1*r1 \le u*u < r2*r2} \lvert F(u,v)\rvert^2$
Angular Sum	$\Phi_{\theta 1,\theta 2} \equiv \sum_{\theta \le (1/tan(\frac{v}{u})) \le \theta 2} \lvert F(u,v)\rvert^2$
Statistical Feature Matrix	
Coarseness	$F_{CRC}=C/\sum_{(i,j)\epsilon Ne} \frac{DSS(i.j)}{n}$
Roughness	$F_{RGH}=(D_f^{(u)}+ D_f^{(v)}/2$
Periodicity	$F_{PER}= (\bar{M}_{dis}-M_{dis}(valley))/M_{dis}$
Contrast	$F_{CON}=[\sum_{(i,j)\epsilon Nr} CON(i,j)/4]^{1/2}$
Co-Occurrence Matrix Based Texture Features	
Angular Second Moment	$f_1=\sum_i \sum_j \{p(i,j)\}^2$
Contrast	$f_2 = \sum_{i=1}^{N-1} n^2 \sum_i \sum_j \{p(i,j)\}$
Correlation	$f_3=(\sum_i \sum_j (i,j)p(i,j) - \mu x * \mu y) / (\sigma x * \sigma y)$
Variance	$f_4=\sum_i \sum_j (i-\mu)^2 p(i,j)$
Inverse Difference Moment	$f_5=\sum_i \sum_j p(i,j)^2/(1+(i-j)^2$
Sum Average	$f_6=\sum_{i=2}^{2Nx} ip_{x+y}(i)$
Sum Variance	$f_7=\sum_{i=2}^{2Nx} (i-f6)p_{x+y}(i)$

4.2 PATTERN RECOGNITION

4.2.1 INTRODUCTION

Pattern can be defined as a structural or quantitative description of an subject of interest. The subject may be a visible object or a system of data. Exploring and analysis of the pattern hence visualized is called *pattern recognition.* A set of patterns which share some properties in common are defined as *pattern class*. For example, we can easily differentiate between trees and animals because they show some distinct properties in common. Hence trees and animals belong to different class.

In a broad sense, we all have been using pattern recognition techniques in our daily life, although without realizing, that is god gifted to us. Every time we see something we try to differentiate objects of similar properties from others without even feeling the complexity behind it. In machine vision field, there are two types of items for recognition:

1) Recognition of concrete items: There are the items that can be visualized easily. Some of them are spatial and temporal properties of objects. For example they are characters of different language, roads, buildings, cars of different colors etc.
2) Recognition of abstract items: It is mainly a conceptual recognition. For example deciding which car is better to purchase, which book is better to refer. This cannot be decided just by some mathematical expression. It depends on the intellectuality of the person and his/her taste. They are totally conceptual. The figure 4.2 shows a typical pattern recognition system.

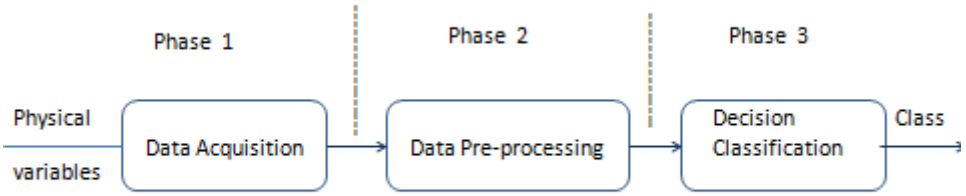

Fig 4.2 Figure showing a conceptual pattern recognition system.

The upcoming sections explain techniques of classification, dimensionality reduction used in our study

4.2.2 DIMENSIONALITY REDUCTION TECHNIQUES

Usually, because of availability of large number of measures and the approach of defining a pattern, the pattern space is of high dimensional. But it does not mean every measure or approach of defining a particular 'object' is useful; sometimes some measures simply reflect some other measure and hence there is overflow of data measured. For considering only the principal measures which can best represent the 'object', there is a need of dimensionality reduction technique. Fisher's Discriminate Ratio (FDR) [18] is one of such widely used techniques in pattern recognition and statistical analysis of data. Some

of the other techniques are – Principal Component Analysis, Factor Analysis, and Independent Component Analysis.

Fisher's Discrimination Ratio (FDR)

Consider two cases shown in figure 4.3. In the first case, the standard deviation within the classes is high and classes slightly overlapping in the feature space. I the second case, the standard deviation is less and class separation is also high. Higher class separation means larger distance between the mean of the classes. Consider the mathematical expression of FDR,

$$FDR = \frac{(\mu 1 - \mu 2)(\mu 1 - \mu 2)}{\sigma 1^2 + \sigma 2^2} \qquad (4.37)$$

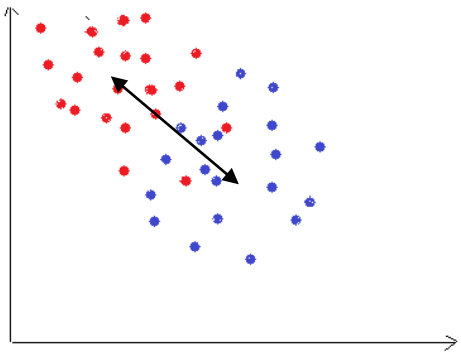

Fig 4.3(a) Case 1 of feature space

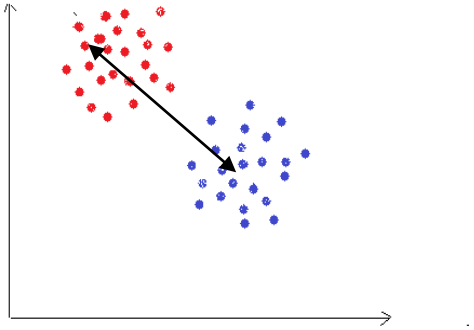

Fig 4.3(b) Case 2 of feature space

it tells that, higher difference between the means, and lower the standard deviation within the higher is the discrimination between the two given classes. Hence higher is the FDR, better is the feature for classification and eventually the respective feature gives better classification accuracy. In case 1, the values are highly scattered around the mean as show in the figure 4.3(a). In case 2, the values are not scattered as much in case 1 and hence gives higher FDR value compared to case 1. Hence feature sets shown in figure 4.3(b) give higher classification accuracy and better discrimination between two classes.

4.2.3 CLASSIFICATION

Classification is a task of training a classification model that maps each attribute set x to one of the predefined class labels y. The figure 4.4 shows a general approach of a classification problem. First, a training set consisting of records whose class labels are known are provided. The training set is then used to train the classification model, which is eventually used to label the testing set.

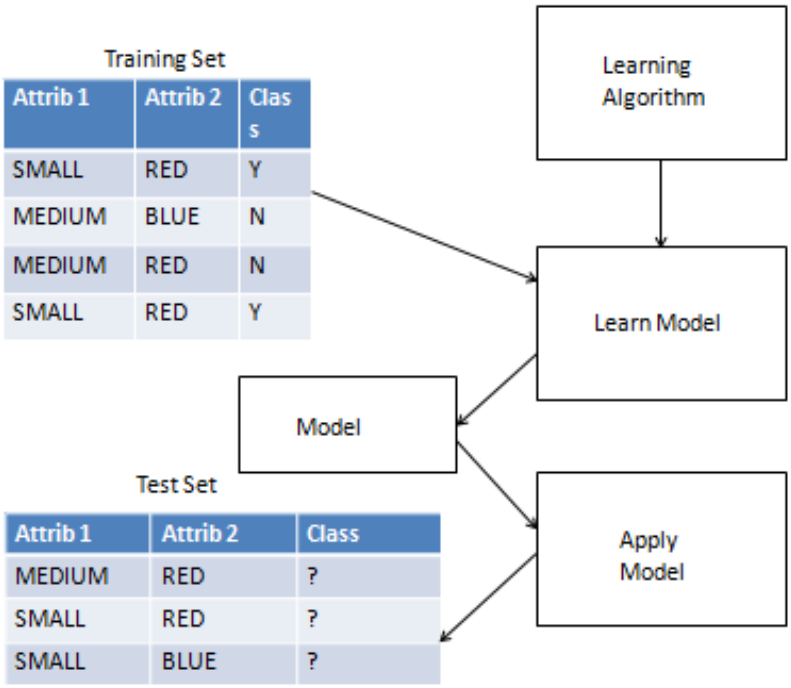

Fig 4.4 Figure showing a general classification approach.

There is no single classification approach which can be used for every problem. A classification model to be chosen is problem specific and accuracy of the result differs from approach to approach. Five classification models, out of which four are in top-ten list of data mining algorithms, are used in our work. They are

1) K-Nearest Neighbor (K-NN)
2) Support Vector Machine
3) Random Forest
4) Decision Tree C 4.5
5) CART(Classification using Regression)

The following sections explain each of them briefly.

4.2.3.1 K-Nearest Neighbor Algorithm (K-NN)

This is one of the oldest, simplest and most popular classification algorithms used in data mining and pattern recognition field. K-NN algorithm [19] tries to find k-nearest points to the testing point and labels(maps) the testing point to a class which appeared maximum number of times in the circle enclosing k-training points. This algorithm is also called as Lazy learning method and it requires very less or no training. The main steps of the algorithms are

1) Define k-value
2) Train the set
3) Distance measurement
4) Labeling.

The figures 4.5(a) and 4.5(b) shows a general approach to label (map, classify) a given data set (point) from a set of predefined labels.

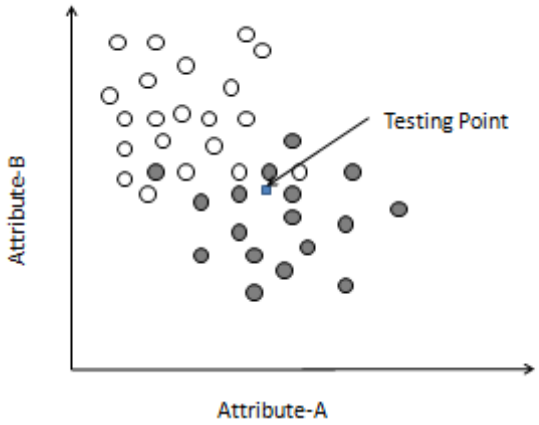

Fig 4.5(a). Figure showing scatter plot of two classes.

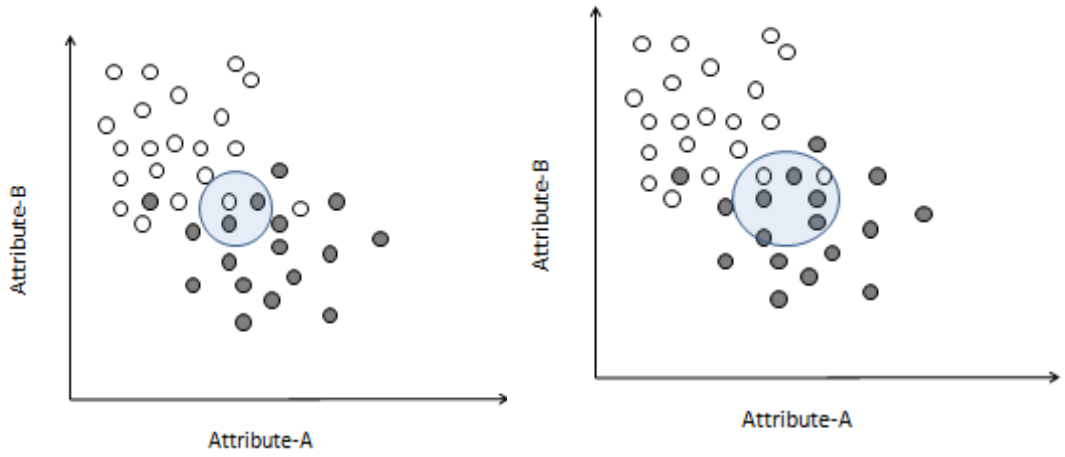

Fig 4.5(b). Figure showing decision making for different k-values

Figure 4.5(a) shows a scatter-plot of two-classes, in which unfilled-'dots ' belong to Class YES and filled-'dots' belong to class NO. The square 'dot' is a point which is to be labeled. Actually the testing dot here belongs to the class YES. Let's see how k-NN algorithm labels the testing set in the following section.

Case1. k=3: Here the value of k is 3, i.e. we are considering 3 nearest points to classify the testing set. We find that out of 3-nearest points, two dots belong to the class NO and one-point belongs to the class YES. Majority is the class NO. Hence the model labels the testing set as class YES.

Case2. k=7: Here the value of k is 7, i.e. we are considering 7 nearest points to classify the testing set. We find that out of 7-nearest points, five dots belong to the class NO and two-point belongs to the class YES. Majority is the class NO. Hence again the model labels the testing set as class NO.

As we have seen, more the number of k-values more the training set it uses for training the model. In the first case the probability of the testing set belonging to class NO was 0.66. But in the second case the probability of labeling the test set to class NO was increased to 0.71, which is more accurate. Hence we can understand a very important fact that, more the value of k more the accurate is the model.

4.2.3.2 Support Vector Machine (SVM)

A standard, binary, SVM [20] takes a set of input data and predicts, for each given input, which of two possible classes forms the input, making the SVM a non-probabilistic binary linear classifier. Given a set of training examples, each marked as belonging to one of two categories, an SVM training algorithm builds a model that assigns new examples into one category or the other. An SVM model is a representation of the examples as points in space, mapped so that the examples of the separate categories are divided by a clear gap that is as wide as possible. New examples are then mapped into that same space and predicted to belong to a category based on which side of the gap they fall on.

In a two-class learning task, the aim of SVM is to find the best classification function to distinguish between members of the two classes in the training data. The metric for the concept of the "best" classification function can be realized geometrically. For a linearly separable dataset, a linear classification function corresponds to a separating hyper-plane $f(x)$ that passes through the middle of the two classes, separating the two. Once this

function is determined, new data instance *xn* can be classified by simply testing the sign of the function

f (xn); *xn* belongs to the positive class if *f (xn)* > 0.

Because there are many such linear hyper-planes, what SVM additionally guarantee is that the best such function is found by maximizing the margin between the two classes. Intuitively, the margin is defined as the amount of space, or separation between the two classes as defined by the hyper-plane. Geometrically, the margin corresponds to the shortest distance between the closest data points to a point on the hyper-plane. Having this geometric definition allows us to explore how to maximize the margin, so that even though there are an infinite number of hyper-planes, only a few qualify as the solution to SVM. To ensure that the maximum margin hyper-planes are actually found, an SVM classifier attempts to maximize the following function with respect to _**w** and *b*:

$$L_p = 1/2\ ||\vec{W}|| - \sum_{i=1}^{t} aiyi(\ \vec{W}.\vec{Xi} + b) + \sum_{i=1}^{t} ai \qquad (4.38)$$

where *t* is the number of training examples, and *αi* , *i* = 1, . . . , *t*, are non-negative numbers such that the derivatives of *L P* with respect to *αi* are zero. *αi* are the Lagrange multipliers and *L P* is called the Lagrangian. In this equation, the vectors _**w** and constant *b* define the hyper-plane. The figure 4.6 shows how the separation-line is drawn and maximization of the margin.

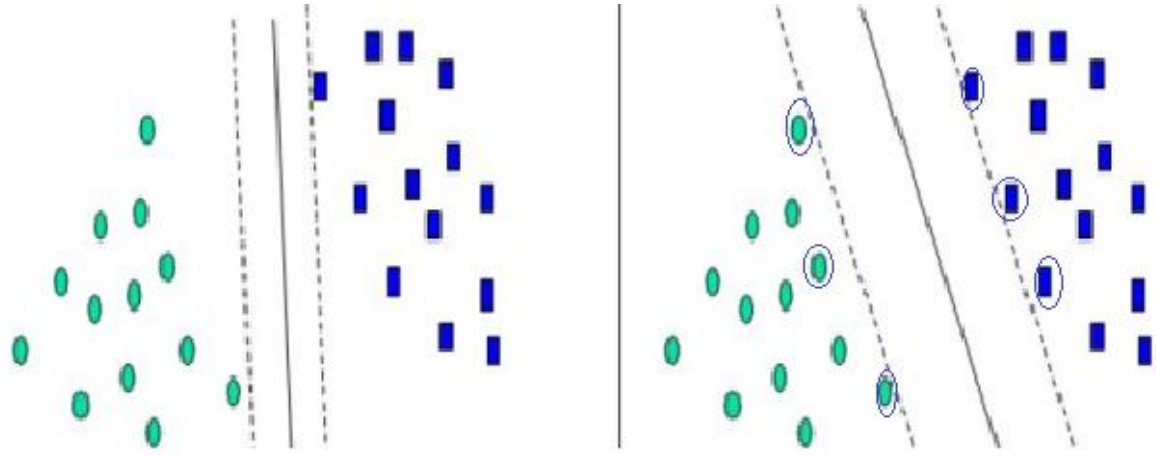

Fig 4.6(a) Fig 4.6(b)

Fig 4.6 Figure showing separation for linear SVM

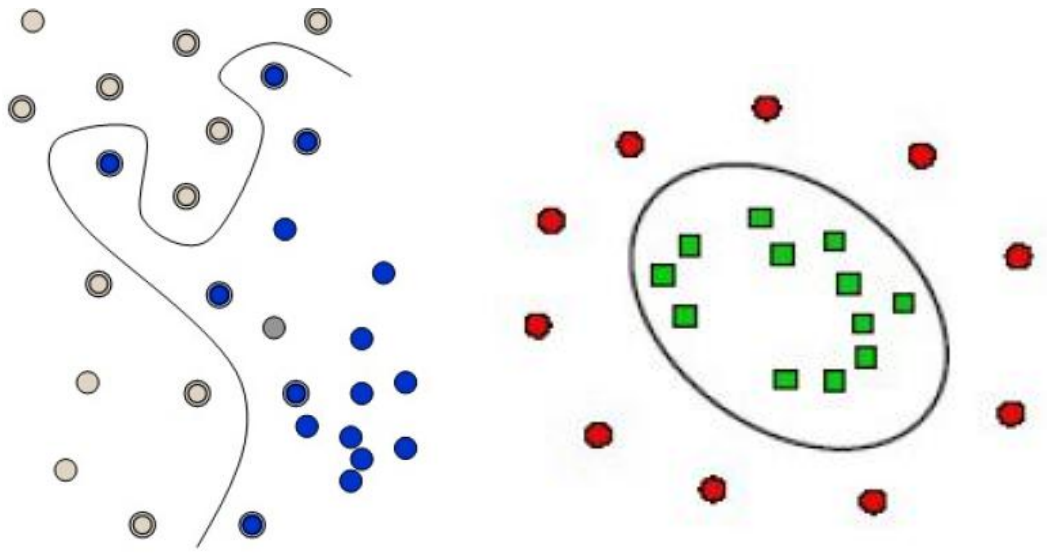

Fig 4.7 Figure showing non-linear dividing line of SVM

The figure 4.6(a) shows that, the margin of separation line is very small and hence it can be proved that generalization error will be high in this case. Figure But the margin in figure 4.6(b) is greater than the margin shown in fig 4.6(a). The encircled dots are the points which actually helps define the margin and those points are called Support Vectors, hence the name Support Vector Machine for this classifier algorithm. Figure 4.7 shows how a hyper-plane is drawn in case non-linear problems.

4.2.3.3 Decision Trees

These are *multistage* decision systems in which classes are sequentially rejected until we reach a finally accepted class. To this end, the feature space is split into unique regions, corresponding to the classes, *in a sequential manner*. Upon the arrival of a feature vector, the searching of the region to which the feature vector will be assigned is achieved via a sequence of decisions along a path of nodes of an appropriately constructed *tree*. Such schemes offer advantages when a large number of classes are involved. The most popular decision trees are those that split the space into hyper-rectangles with sides parallel to the axes. The sequence of decisions is applied to individual features, and the questions to be answered are of the form "*is feature xi* $\leq \alpha$?" where α is a threshold value. Such trees are known as *ordinary binary classification trees (OBCTs)*. Other types of trees are also possible that split the space into convex polyhedral cells or into pieces of spheres. The basic idea behind an OBCT is demonstrated via the simplified example of Figure 4.8. Figure 4.8 shows the respective binary tree with its decision nodes and leaves.

The task illustrated in Figure 4.8 is a simple one in the two-dimensional space. The thresholds used for the *binary splits* at each node of the tree in Figure 4.8 were dictated by a simple observation of the geometry of the problem. However, this is not possible in higher dimensional spaces. Furthermore, we started the queries by testing $x1$ against 1/4. An obvious question is why to consider $x1$ first and not another feature. In the general case, in order to develop a binary decision tree, the designer has to consider the following design elements in the training phase:

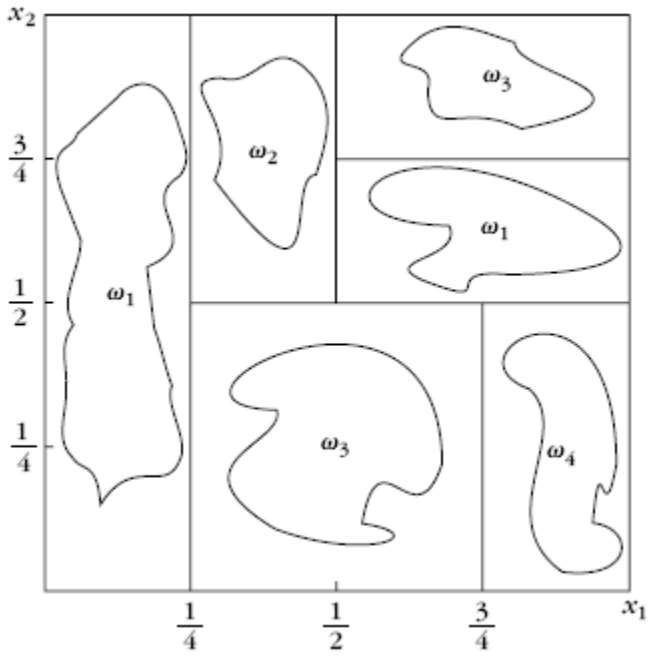

Fig 4.8 Figure showing a two dimensional space and class regions.

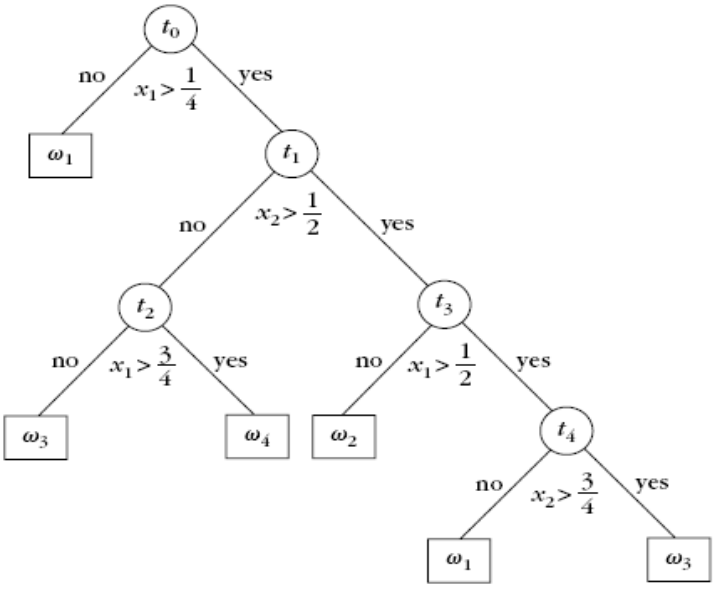

Fig 4.9 Figure showing decision tree.

- At each node, the set of candidate questions to be asked has to be decided. Each question corresponds to a specific binary split into two descendant nodes. Each node, t, is associated with a specific subset Xt of the training set X. Splitting of a node is equivalent to the split of the subset Xt into two disjoint descendant subsets, Xty , Xtn . The first of the two consists of the vectors in Xt that correspond to the answer "Yes" of the question and those of the second to the "No." The first (root) node of the tree is associated with the training set X. For every split, the following is true:

$$X_{ty} \cap X_{tn} \neq 0 \quad (4.39)$$

$$X_{ty} \cap X_{tn} = X_t \quad (4.40)$$

- A *splitting criterion* must be adopted according to which the best split from the set of candidate ones is chosen.
- A stop-splitting rule is required that controls the growth of the tree, and a node is declared as a terminal one (*leaf).*
- A rule is required that assigns each leaf to a specific class.

Random Forest

Random forest [21,22] is a type of recursive partitioning decision tree method which involve an ensemble of classification (or regression) trees that are calculated on random subsets of the data, using a subset of randomly restricted and selected predictors for each split in each classification tree In this way, random forests are able to better examine the contribution and behaviour that each predictor has, even when one predictor's effect would usually be overshadowed by more significant competitors in simpler models (e.g., simple or mixed effect regression models). Furthermore, the results of an ensemble of classification/regression trees have been shown to produce better predictions than the results of one classification tree on its own.

C 4.5

C4.5 [23] builds decision trees from a set of training data using the concept of information entropy. The training data is a set $S = s_1, s_2, \cdots$of already classified samples. Each sample $s_i = x_1, x_2, \cdots$is a vector where $x_1, x_2, \cdots$represent attributes

or features of the sample. The training data is augmented with a vector $C = c_1, c_2, \ldots$ where $c_1, c_2, \cdots$represent the class to which each sample belongs.

At each node of the tree, C4.5 chooses one attribute of the data that most effectively splits its set of samples into subsets enriched in one class or the other. Its criterion is the normalized information gain (difference in entropy) that results from choosing an attribute for splitting the data. The attribute with the highest normalized information gain is chosen to make the decision. The C4.5 algorithm then recourses on the smaller sub lists.

4.2.4 CLASSIFIER ENSEMBLES

Another trend that offers more possibilities to the designer is to *combine different Classifiers*. Thus, one can exploit their individual advantages in order to reach an overall better performance than could be achieved by using each of them separately. An important observation that justifies such an approach is the following. From the different (candidate) classifiers we design in order to choose the one that fits our needs, one results in the best performance; that is, minimum classification error rate. However, different classifiers may fail (to classify correctly) on different patterns. That is, even the "best" classifier can fail on patterns that other classifiers succeed on. A schematic classifier combiner is shown in the figure 4.10.

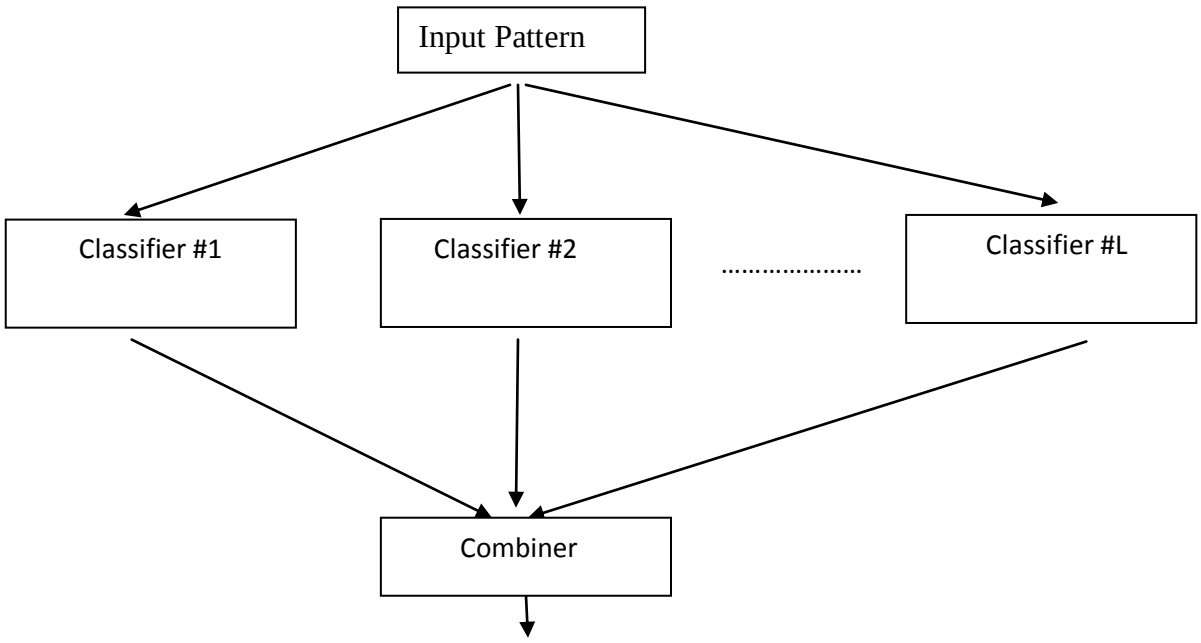

Figure 4.10 A schematic classifier combiner

Combining classifiers aims at exploiting this complementary information that seems to reside in the various classifiers. The results of the individual classifiers are then combined using a rule. There are many rules which make possible a efficient ensemble. Majority voting is the simplest methods of all. This is explained here below.

4.2.4.1 Majority Voting Rule:

Majority voting rule [24] is one of the simplest and robust schemes. According to the majority vote scheme, one decides in favour of the class for which there is a consensus, or when at least *lc* of the classifiers agree on the class label of the unknown pattern, where

$$I_c = \begin{cases} \frac{L}{2} + 1, L\ even \\ \frac{L+1}{2}, L\ odd \end{cases} \quad (4.41)$$

Otherwise, the decision is *rejection.* In other words, the combined decision is correct when the decisions of the majority of classifiers are correct, and it is wrong when the decisions of the majority of classifiers are wrong and they *agree* on the wrong label. A rejection is considered neither correct nor wrong.

Implementation

In this work, all the pattern recognition algorithms mentioned here are used for classification. The classifiers, initially, are used individually for every possible combination of best-selected feature set of two and their accuracies and precisions are calculated. The k-NN classifier with different k-values is tested and it is found that k-value of five gives better result. Cross-validation value of ten is used so that every dataset set used for training as well as testing. Even though some classifiers outperform other classifiers, the later classifiers are used by classifier combiners.

CHAPTER-5
RESULTS

This chapter deals with the results of the work at various levels. The results presented are,

1) Texture feature extraction
2) Data preprocessing (Dimensionality reduction)
3) Classification
4) Classification combiner

5.1 FEATURE EXTRACTION

The texture features are measured for four classes, namely – Normal, Acute, Chronic, and Hemorrhage. In a total 26 texture measurements are extracted which are are presented in the table 5.1 to 5.4. By a simple observation of the tables for the different classes, we can see that the measured values abruptly change from class to class. This is more prominent when there is a large visual difference between the classes, such as chronic and hemorrhage. The characteristics of acute and chronic classes are similar which makes the analysis more difficult. The tables show extracted measurements for a total 91 cases belonging to different symptoms.

Table 5.1 Table showing extracted texture measurements for the class Acute

Energy	0.094102	0.093516	0.089567	0.081031	0.087263	0.087397	0.075673	0.073791	0.070768	0.072341	0.069873	0.062448
FRACTAL1	0.345044	0.33046	0.303757	0.35256	0.390652	0.391295	0.36097	0.376619	0.385656	0.399741	0.398095	0.350005
FRACTAL2	0.134819	0.11402	0.019247	0.123743	0.126402	0.20133	0.179226	0.234661	0.247064	0.253079	0.263445	0.127486
Angular Sum	108.9404	117.5883	135.9154	161.8116	167.2379	154.7546	181.6287	133.2817	176.2796	148.9094	129.0794	163.461
Coars_SFM	13.4711	11.493	10.53664	8.308106	8.450799	8.522513	7.977173	9.768732	9.527711	10.38659	11.13677	8.760923
Contrast_GLDM	37.61768	55.92134	69.59939	93.94024	84.73902	84.08354	107.6134	60.28902	60.55976	48.59817	42.28049	82.04695
Contrast_SFM	8.701426	10.60717	11.83533	13.75239	13.06041	13.00989	14.71607	11.01418	11.03923	9.891437	9.223834	12.85408
Energy_GLDM	0.141525	0.113679	0.101829	0.114111	0.121194	0.124758	0.102926	0.114569	0.113673	0.12114	0.130784	0.101043
Entropy	2.514403	2.509028	2.585548	2.651882	2.576634	2.598718	2.73422	2.741988	2.786873	2.710025	2.745737	2.915271
Entropy_GLDM	2.159286	2.3751	2.487575	2.408414	2.33222	2.335454	2.462347	2.376773	2.383512	2.30101	2.225207	2.521111
Homogeneity GLDM	0.234229	0.195578	0.174403	0.170985	0.167345	0.176075	0.162686	0.172343	0.172366	0.195628	0.208661	0.147156
Kurtosis	2.692167	2.673902	3.483718	2.735599	2.736056	3.296833	3.211437	2.57134	2.592909	2.240506	2.20011	2.958565
M	1.009621	1.008426	1.008004	1.005964	1.007303	1.007439	1.009321	1.012526	1.015063	1.013528	1.013874	1.015187
Mean	70.04989	72.37415	76.26757	125.356	105.7846	106.0998	107.8209	77.9932	76.80499	76.31973	78.71429	86.64399
Mean_GLDM	4.775	5.843293	6.557927	7.486585	7.213415	7.011585	8.160976	6.171951	6.190244	5.490854	5.108537	7.210366
Median	69.19531	71.475	76.75893	124.4528	104.9914	105.4035	107.9057	79.01042	78.55102	77.04651	79.13953	86.75676
Period_SFM	0.482966	0.408384	0.406687	0.560857	0.484501	0.528421	0.506365	0.491096	0.489133	0.524937	0.506535	0.528996
Radial Sum	1476.293	1524.396	1605.753	2638.035	2226.088	2233.876	2271.691	1645.636	1617.852	1608.804	1661.463	1829.164
Roughness_SFM	2.538046	2.571597	2.630979	2.515228	2.473874	2.439569	2.524012	2.480907	2.461672	2.435707	2.420472	2.53474
Skewness	0.141538	-0.21033	0.277355	-0.24026	0.095929	-0.24068	-0.30579	-0.2563	-0.20516	0.020968	-0.1406	0.139211
TEM1	17180.04	18040.41	16987.56	22246.19	24491.47	25208.41	27388.93	25935.78	32405.77	25660.79	27989.46	28439.8
TEM2	959.2457	1112.651	1096.819	1331.617	1537.898	1766.823	1314.592	1172.302	1269.524	1091.117	925.7499	1243.571
TEM3	208.3254	220.9875	272.8767	290.4656	331.221	313.7443	304.3675	270.224	262.5685	223.0777	197.3034	257.0278
TEM4	4154.892	4572.475	4888.855	6522.129	6645.718	7014.575	6039.763	5854.91	6238.231	5732.65	4981.741	6108.291
TEM5	461.0949	482.4301	564.2214	598.8216	736.07	731.8573	652.3335	517.9541	526.5419	496.8214	428.8158	597.7729
TEM6	1894.852	2225.875	2704.929	2889.123	3123.763	3074.455	2991.921	2186.498	2401.034	2360.532	1826.685	2740.556

Table 5.1 continued

Energy	0.079303	0.079149	0.082892	0.074696	0.085073	0.087798	0.081586	0.084507	0.071508	0.068403	0.062479	0.074079	0.064556
FRACTAL1	0.318438	0.36967	0.40154	0.409445	0.359983	0.371045	0.318643	0.343363	0.361838	0.37796	0.383365	0.410462	0.347682
FRACTAL2	0.076033	0.156369	0.161151	0.204467	0.131935	0.142883	0.045894	0.131571	0.16959	0.257132	0.227382	0.236392	0.085715
Angular Sum	142.8338	139.1169	142.1566	140.7551	147.6939	144.1718	142.1935	164.5828	180.866	151.1837	186.086	132.3102	166.0422
Coars_SFM	10.29708	10.59376	10.22147	9.699229	8.601618	8.700239	10.27594	8.955288	8.151393	9.468086	9.294144	10.59334	8.689827
Contrast_GLDM	75.16402	58.89329	55.87317	64.05549	85.86341	83.21341	69.15854	79.53537	99.11098	63.50427	64.25915	44.7122	86.05732
Contrast_SFM	12.29947	10.88636	10.60509	11.35433	13.14626	12.94298	11.79691	12.65343	14.12338	11.30438	11.37133	9.487878	13.16416
Energy_GLDM	0.099168	0.114059	0.118074	0.110611	0.122133	0.119367	0.107238	0.123615	0.109278	0.110221	0.11048	0.126553	0.098038
Entropy	2.710258	2.678752	2.64817	2.741455	2.610366	2.585158	2.650271	2.64058	2.72308	2.822145	2.898799	2.689051	2.883802
Entropy_GLDM	2.508882	2.379865	2.351313	2.417328	2.355824	2.335861	2.43184	2.330432	2.397372	2.407731	2.407634	2.264341	2.545752
Homogeneity GLDM	0.176604	0.193886	0.205575	0.188616	0.177515	0.18928	0.179287	0.172107	0.156253	0.167894	0.171196	0.203159	0.145464
Kurtosis	3.347702	2.734522	2.96145	2.774963	2.755976	2.89427	2.670142	2.998815	2.246818	2.698909	2.48833	2.220689	3.036779
M	1.006505	1.012177	1.013697	1.015468	1.005328	1.007297	1.010706	1.005866	1.009491	1.01602	1.020934	1.013653	1.013803
Mean	104.1995	70.44671	67.6576	70.19728	125.9048	105.873	72.43084	127.678	110.1156	76.68707	73.65533	76.13152	85.67347
Mean_GLDM	6.69939	5.989634	5.8	6.210366	7.120732	7.079268	6.568293	6.936585	7.921951	6.334756	6.359146	5.263415	7.389024
Median	104.3617	69.42391	66.15323	69.27632	127.6744	105.1385	73.525	128.1389	111.5143	78.59574	74.10811	76.97561	84.40789
Period_SFM	0.424344	0.450638	0.502069	0.492638	0.559065	0.473428	0.421367	0.525796	0.49539	0.487822	0.499001	0.551548	0.517715
Radial Sum	2193.255	1485.363	1426.311	1482.102	2649.627	2229.551	1526.067	2686.163	2319.61	1619.095	1554.584	1605.947	1807.549
Roughness_SFM	2.59301	2.496827	2.443105	2.424923	2.506981	2.508666	2.589022	2.527556	2.5103	2.462442	2.44239	2.417933	2.553671
Skewness	-0.22491	0.110784	0.372608	0.07078	-0.25464	-0.07986	0.060716	-0.12551	-0.02975	-0.29588	-0.118	0.036318	0.166498
TEM1	20611.41	17585.35	21503.81	19746.98	24413.55	23385.93	18229.44	27733.55	29390.54	29504.53	35600.16	27585.37	29123.69
TEM2	1254.059	1282.426	1476.349	1535.142	1300.929	1441.95	1024.428	1124.724	1699.11	1309.011	1339.299	1055.326	1255.602
TEM3	276.5419	255.9792	267.5195	272.2495	286.7418	280.3709	264.1787	268.3281	320.7483	275.1189	298.7925	217.338	274.9827
TEM4	4586.833	5030.571	5875.743	5613.723	6458.281	6403.658	4827.986	6053.263	6521.745	6270.752	6112.536	5832.846	5748.646
TEM5	590.3436	576.4144	643.344	634.0215	598.3703	648.2141	521.1329	549.4257	739.7353	532.3363	575.5406	477.8658	596.0061
TEM6	2312.839	2212.442	2605.218	2388.944	2949.738	3064.935	2415.349	2882.835	2724.656	2225.735	2290.97	2242.75	2875.546

Table 5.2 Table showing extracted texture measurements for the class Normal.

Energy	0.082687	0.074264	0.06904	0.080918	0.08208	0.080486	0.077833	0.071303	0.077308	0.079211	0.074161	0.066572	0.081525
FRACTAL1	0.373352	0.331148	0.364761	0.359062	0.390963	0.387112	0.341351	0.331849	0.323885	0.371747	0.379241	0.387274	0.38496
FRACTAL2	0.253798	0.124911	0.202428	0.166417	0.117083	0.12056	0.174478	0.127765	0.059914	0.223965	0.162525	0.17437	0.131982
Angular Sum	128.1484	164.5342	151.2316	180.9931	158.8065	173.4474	196.8464	136.3158	143.5287	139.1726	143.6402	157.8845	153.3558
Coars_SFM	12.7076	10.61787	9.645343	9.061867	8.403922	8.899511	8.639458	9.648543	10.6198	11.20345	9.496137	9.980749	10.45526
Contrast_GLDM	35.29756	67.64451	68.40549	81.09512	88.09329	78.80549	94.48963	73.44573	63.34146	49.82622	68.0378	59.13659	59.95671
Contrast_SFM	8.429438	11.66812	11.73428	12.77582	13.31571	12.59498	13.7921	12.15819	11.29017	10.01423	11.70405	10.91114	10.98673
Energy_GLDM	0.146763	0.105299	0.107107	0.122699	0.114438	0.125877	0.114587	0.10555	0.108883	0.120448	0.106417	0.112254	0.110698
Entropy	2.667426	2.755554	2.815389	2.665018	2.673963	2.677116	2.69285	2.768255	2.695977	2.65825	2.685595	2.818019	2.674257
Entropy_GLDM	2.131123	2.466403	2.448437	2.338435	2.388439	2.310207	2.400013	2.487131	2.430029	2.313534	2.461024	2.38923	2.411706
Homogeneity GLDM	0.219902	0.179808	0.175172	0.190152	0.17426	0.18021	0.158734	0.166688	0.187092	0.19968	0.169827	0.189191	0.194862
Kurtosis	3.221564	3.000184	2.819987	3.059914	3.022862	3.054198	3.018366	2.661132	2.801161	2.480391	2.282662	2.365623	3.027955
M	1.008269	1.008955	1.008936	1.004624	1.00485	1.005055	1.00507	1.007276	1.006327	1.006655	1.007003	1.008249	1.006151
Mean	90.65079	90.97732	98.03175	143.4875	142.61	140.0068	144.5964	100.3741	101.381	97.65079	97.69161	105.9615	104.102
Mean_GLDM	4.623171	6.468902	6.534756	7.010976	7.393293	6.931098	7.644512	6.675	6.2	5.514024	6.491463	6.052439	5.97622
Median	91.65854	91.65476	98.72619	142.6848	142.8	139.7813	143.2841	99.35	101.85	97.4	98.63542	105.4043	104.7283
Period_SFM	0.515599	0.461775	0.462846	0.511306	0.511972	0.516036	0.449132	0.485871	0.467493	0.497179	0.552551	0.506903	0.478233
Radial Sum	1909.015	1914.744	2065.14	3017.097	3000.234	2944.771	3040.203	2114.126	2133.328	2054.914	2056.216	2231.096	2189.441
Roughness_SFM	2.463365	2.570583	2.502853	2.528073	2.482915	2.466604	2.539546	2.575134	2.603159	2.472867	2.490271	2.446202	2.493896
Skewness	-0.14571	-0.14238	-0.2004	0.452122	-0.0071	0.093369	0.113302	-0.17899	0.151819	-0.13005	-0.12981	-0.00767	0.174234
TEM1	21396.94	24219.18	23866.22	21858.22	22002.07	25905.58	32768.66	24320.58	25103.64	22547.73	22358.8	27176.9	22909.4
TEM2	889.2885	1148.471	1294.695	1400.877	1553.734	1384.499	1439.556	1090.836	1015.073	1065.26	1215.157	1336.3	1261.498
TEM3	150.6069	265.473	281.4068	313.6528	355.0744	271.8262	325.373	256.8025	274.6167	211.0569	215.7625	239.2047	238.318
TEM4	4653.14	4167.266	5577.894	6149.039	6567.562	5860.255	5980.029	5410.052	4721.654	5061.191	5819.254	5644.696	4922.375
TEM5	373.5241	560.0182	597.6505	648.6924	737.6854	610.143	665.9031	514.1905	520.5422	453.5341	529.1733	573.0584	582.8705
TEM6	1912.459	2220.392	2474.633	2576.754	2769.138	2470.403	2658.757	2496.561	2265.102	2043.214	2641.746	2202.008	2436.309

Table 5.2 Continued

Energy	0.082892	0.074203	0.075529	0.06614	0.068958
FRACTAL1	0.40154	0.362924	0.361233	0.348987	0.394256
FRACTAL2	0.161151	0.134515	0.141582	0.200584	0.21758
Angular Sum	142.1566	142.8986	145.2911	183.9416	222.1025
Coars_SFM	10.22147	9.632407	9.325808	8.096891	8.291039
Contrast_GLDM	55.87317	72.33354	74.63841	95.60549	84.18963
Contrast_SFM	10.60509	12.06739	12.25889	13.87183	13.01883
Energy_GLDM	0.118074	0.102715	0.10204	0.110674	0.11771
Entropy	2.64817	2.751852	2.753743	2.871133	2.781293
Entropy_GLDM	2.351313	2.493771	2.503992	2.429221	2.333162
Homogeneity GLDM	0.205575	0.173026	0.162683	0.165644	0.171874
Kurtosis	2.96145	2.910564	3.108391	2.95713	2.566946
M	1.013697	1.006382	1.006289	1.007839	1.008658
Mean	67.6576	107.6893	111.2336	142.5805	127.5669
Mean_GLDM	5.8	6.653049	6.788415	7.667683	7.239634
Median	66.15323	107.1146	111.5341	142.6744	127.9219
Period_SFM	0.502069	0.470447	0.559911	0.524597	0.538071
Radial Sum	1426.311	2266.529	2341.022	3003.05	2683.561
Roughness_SFM	2.443105	2.525711	2.536844	2.518682	2.448195
Skewness	0.372608	0.098506	0.046113	0.224391	0.143717
TEM1	21503.81	23350.2	26199.44	36557.4	42985.54
TEM2	1476.349	1487.828	1095.092	1289.549	1487.771
TEM3	267.5195	313.8021	208.8998	313.5537	293.9522
TEM4	5875.743	5772.087	5989.786	6415.643	6951.966
TEM5	643.344	681.8139	499.9206	649.7005	672.83
TEM6	2605.218	2754.459	2629.931	2872.177	2959.752

Table 5.3 Table showing extracted texture measurements for the class Chronic.

Energy	0.042991	0.067302	0.04803	0.04332	0.081998	0.046807	0.082265	0.093022	0.0828	0.039464	0.05634	0.062572
FRACTAL1	0.400479	0.297724	0.411614	0.462643	0.362693	0.408495	0.354307	0.293074	0.292362	0.4728	0.33832	0.387558
FRACTAL2	0.328831	0.20007	0.345114	0.294371	0.108387	0.201504	0.136998	0.080003	0.065509	0.32624	0.17009	0.234435
Angular Sum	214.335	204.2768	339.3737	397.7989	128.8061	160.4276	182.9959	143.675	161.3598	271.2886	155.9199	227.3994
Coars_SFM	6.079843	7.571637	6.219075	5.139356	10.93198	7.882778	8.543925	9.336532	8.361811	5.701595	8.516453	6.531764
Contrast_GLDM	131.4671	133.6073	137.9677	146.203	58.24207	76.63232	99.2378	94.5622	121.2701	119.9341	93.48841	129.4622
Contrast_SFM	16.27264	16.39529	16.66414	17.16126	10.82678	12.42097	14.13065	13.79179	15.62143	15.54448	13.71624	16.14854
Energy_GLDM	0.09441	0.097429	0.091912	0.09144	0.110332	0.098851	0.113957	0.108047	0.098771	0.112916	0.091153	0.099896
Entropy	3.241822	2.870111	3.161767	3.298707	2.648597	3.184638	2.635061	2.524093	2.635337	3.322967	3.058884	2.925708
Entropy_GLDM	2.545494	2.544408	2.595972	2.614347	2.396119	2.511831	2.411115	2.425747	2.50804	2.496535	2.61846	2.553176
Homogeneity GLDM	0.145716	0.140516	0.146259	0.134704	0.178853	0.171885	0.175096	0.155275	0.149716	0.159548	0.152903	0.150991
Kurtosis	2.003558	3.045497	3.013549	2.784532	2.93074	2.963151	2.774244	2.881616	2.830083	2.253493	3.829257	2.822446
M	1.0717	1.028584	1.032693	1.061348	1.019443	1.071127	1.037624	1.033244	1.030251	1.169165	1.091701	1.085099
Mean	79.90703	70.17914	96.34467	92.96599	52.89569	55.61224	48.6712	42.22222	50.93424	54.47619	42.20181	45.84354
Mean_GLDM	9.042683	9.106098	9.089634	9.412805	6.035976	6.878659	7.69878	7.739024	8.688415	8.381707	7.511585	8.776829
Median	77.32143	69.82979	96	98.77419	53.7234	54.14063	48.42857	41.37963	51.07547	52.825	41.07813	47.67045
Period_SFM	0.545749	0.436634	0.509433	0.65395	0.47969	0.58972	0.470683	0.415578	0.377244	0.61555	0.466708	0.608561
Radial Sum	1728.54	1488.521	2036.493	1974.075	1119.029	1204.702	1032.334	898.5808	1082.767	1214.893	923.7575	985.4666
Roughness_SFM	2.407926	2.585772	2.38478	2.313196	2.540841	2.417936	2.539334	2.648034	2.633503	2.270608	2.556596	2.433756
Skewness	0.197918	0.014315	0.332983	-0.67273	0.123477	0.483335	-0.19765	-0.11496	0.03394	0.300208	0.701407	-0.0121
TEM1	60165.14	35721.56	44570.45	83124.12	16076.58	30731.72	28133.35	18192.71	19314.37	58557.75	26328.27	38140.79
TEM2	1374.53	1498.777	2330.077	2005.973	1141.404	1049.509	1350.696	1340.091	1453.109	1692.131	1376.128	1823.828
TEM3	281.605	341.6033	404.8247	382.5206	265.9233	234.1866	311.6726	312.5905	348.4747	241.2275	309.6508	291.4328
TEM4	8400.584	6558.898	9481.426	11502.12	4524.496	6947.113	6061.071	5118.786	5488.034	10407.91	5587.963	8969.524
TEM5	623.9943	714.5068	892.6226	833.2222	553.9478	510.1325	635.55	653.7466	717.2239	589.4345	639.5151	778.8395
TEM6	2749.687	2895.467	3206.439	3807.635	2258.75	2185.129	2925.413	2707.687	2792.596	3091.146	2292.402	3982.664

Table 5.3 Continued

Energy	0.073113	0.066459	0.07666	0.073277	0.043403	0.071508	0.046909	0.066675	0.045459	0.064053	0.07049	0.081031	0.076825
FRACTAL1	0.391156	0.39194	0.359287	0.390509	0.411397	0.327174	0.413794	0.372318	0.36414	0.40838	0.382871	0.29792	0.310738
FRACTAL2	0.207258	0.199951	0.163717	0.157241	0.326412	0.024057	0.280406	0.11229	0.243338	0.192885	0.106595	0.106932	0.103756
Angular Sum	151.898	171.1841	149.8649	180.5021	230.4355	204.0025	222.7106	181.4153	240.3497	212.1803	172.4558	176.689	208.2655
Coars_SFM	8.172685	7.775079	10.42196	8.2865	6.056787	7.256543	8.125992	10.23649	7.507417	6.145764	8.276863	8.685639	8.289795
Contrast_GLDM	91.07256	96.62012	61.68049	89.30427	124.8134	149.1207	71.55854	60.28049	96.02317	140.3024	89.74085	107.8585	108.9098
Contrast_SFM	13.54291	13.94897	11.1412	13.41087	15.85543	17.32316	12.00249	11.0169	13.9029	16.81078	13.44244	14.7341	14.8021
Energy_GLDM	0.095792	0.091496	0.110058	0.096657	0.098176	0.088905	0.102613	0.111537	0.087818	0.095196	0.095863	0.103606	0.109649
Entropy	2.810258	2.883644	2.723496	2.808309	3.233095	2.820541	3.158688	2.872126	3.287629	2.932488	2.823105	2.649409	2.718757
Entropy_GLDM	2.596379	2.639282	2.420814	2.582462	2.520106	2.635497	2.467153	2.404117	2.640261	2.594594	2.588693	2.46594	2.425127
Homogeneity GLDM	0.1585	0.145012	0.185783	0.161131	0.151865	0.135626	0.175774	0.190403	0.144239	0.142496	0.159193	0.13796	0.161689
Kurtosis	3.54661	3.195283	3.032942	3.490581	1.986965	3.845655	2.34816	3.153292	2.974081	3.34029	3.142458	2.991509	2.88998
M	1.07703	1.088532	1.065377	1.074241	1.070105	1.044574	1.069408	1.024078	1.143377	1.06831	1.067504	1.046642	1.038525
Mean	33.86621	33.92744	32.55556	34.41043	80.22449	51.03175	55.65306	64.51701	46.75964	49.36054	35.81859	44.42857	53.17914
Mean_GLDM	7.389634	7.685976	6.096341	7.293293	8.736585	9.518293	6.662195	6.035366	7.712195	9.193902	7.333537	8.35122	8.118293
Median	33.10638	33.01136	32.63415	33.28571	79.84211	50.69231	54.44643	63.875	42.73611	48.44048	35.65116	44.94118	53.87273
Period_SFM	0.568404	0.562559	0.522079	0.553318	0.552807	0.464744	0.581124	0.54082	0.506298	0.623791	0.552261	0.427161	0.442807
Radial Sum	730.9131	731.9754	696.3918	735.4917	1732.196	1089.895	1191.597	1363.926	1033.976	1064.455	766.9922	945.5898	1126.283
Roughness_SFM	2.444181	2.435025	2.510317	2.450655	2.373942	2.583391	2.408421	2.494087	2.485831	2.409084	2.465085	2.645495	2.598235
Skewness	0.325868	0.301684	-0.01613	0.284899	0.134621	0.434949	0.21788	0.419777	0.775627	0.189185	0.264656	0.058994	-0.11244
TEM1	25859.54	29475.17	23823.37	24606.39	58937.8	21534.75	50885.21	19299.95	38497.24	33542.81	24502.25	25289.13	29974.34
TEM2	1982.284	1970.271	1077.364	1901.213	1460.992	1669.031	1210.171	1186.824	1339.399	1800.505	1808.429	1532.226	1605.192
TEM3	327.731	329.8806	226.188	317.9741	298.623	433.5532	258.8195	223.9345	304.2862	269.6679	288.5985	325.7855	363.1399
TEM4	7809.104	7973.589	4814.496	7609.822	9763.83	6403.635	7181.164	4723.38	6612.939	8853.168	7237.999	5691.199	6435.025
TEM5	815.3775	813.8759	473.327	788.0531	671.2408	867.071	560.72	526.4975	618.0136	739.4061	736.3802	720.0015	747.3557
TEM6	3518.67	3544.335	1886.108	3388.993	2989.294	3517.937	2494.196	2245.735	2260.541	3966.515	3312.3	2865.671	3015.09

Table 5.4 Table showing extracted texture measurements for the class Hemorrhage.

Energy	0.064005	0.094366	0.050869	0.050375	0.066667	0.067652	0.060011	0.048894	0.051455
FRACTAL1	0.30969	0.229265	0.361753	0.356179	0.32048	0.399232	0.357076	0.361576	0.376271
FRACTAL2	0.177992	0.14321	0.172142	0.171575	0.173314	0.168206	0.155542	0.232858	0.219452
Angular Sum	1153.287	865.6556	278.5247	220.2635	937.2274	156.1105	179.9125	239.1318	185.0797
Coars_SFM	6.997237	8.774649	6.551651	6.519396	6.774973	9.435525	8.560693	7.839059	6.985425
Contrast_GLDM	142.3931	121.1558	150.3646	151.6841	145.4386	64.89512	81.0128	91.47134	103.864
Contrast_SFM	16.95225	15.64371	17.39842	17.47459	17.14846	11.43002	12.77024	13.57016	14.46477
Energy_GLDM	0.089528	0.094562	0.073494	0.072945	0.090013	0.112784	0.100251	0.092917	0.089993
Entropy	2.913045	2.480272	3.16388	3.170626	2.868598	2.866054	2.969813	3.10531	3.109765
Entropy_GLDM	2.625186	2.551213	2.839722	2.849696	2.6204	2.398412	2.535129	2.608782	2.621504
Homogeneity GLDM	0.146952	0.156679	0.136548	0.125444	0.142646	0.175038	0.158856	0.147345	0.137032
Kurtosis	3.002918	4.262016	3.615504	3.537137	4.336093	5.031635	3.423296	2.142979	2.656617
M	1.00523	1.001626	1.006344	1.006431	1.004372	1.003737	1.003624	1.007212	1.006176
Mean	228.8399	236.6649	181.6372	181.4853	229.8281	158.7551	182.0862	158.4762	160.3583
Mean_GLDM	9.179231	8.579935	9.454878	9.558537	9.407135	6.264634	7.070122	7.568902	8.122561
Median	233.2321	236.4904	184.1724	184.0536	232.8966	159.6744	183.7206	157.8095	160.8182
Period_SFM	0.475413	0.361096	0.553864	0.557147	0.501985	0.562821	0.549341	0.527043	0.601664
Radial Sum	1942.466	2726.444	3819.292	3820.083	1629.925	3338.964	3828.993	3333.591	3376.013
Roughness_SFM	2.534996	2.690107	2.508346	2.520933	2.503092	2.444973	2.476781	2.475465	2.444788
Skewness	-0.85248	-0.8721	-0.75925	-0.72151	-1.04832	-0.77641	-0.56685	0.143503	-0.17516
TEM1	47330.24	4275.046	45701.73	46723.36	21602.71	21095.89	25399.13	47493.23	35163.68
TEM2	2296.692	927.8011	1589.309	1602.614	1080.924	1205.434	1184.018	1401.954	1471.826
TEM3	472.9973	257.9284	398.0438	383.8651	294.2069	248.7	258.1994	258.8275	254.7995
TEM4	6895.683	1889.95	8377.371	8422.891	7060.411	5851.675	6167.607	7507.477	7956.894
TEM5	1004.852	455.6973	795.9783	775.1799	513.7893	545.6418	541.693	598.4295	590.4898
TEM6	2737.847	1527.37	3518.775	3565.015	2743.177	2328.466	2538.897	2811.328	3074.89

Table 5.4 Continued

Energy	0.092351	0.054046	0.054046	0.060371	0.043269	0.050375
FRACTAL1	0.312504	0.361635	0.361635	0.358552	0.403558	0.356179
FRACTAL2	0.155121	0.210272	0.210272	0.173383	0.258244	0.171575
Angular Sum	1067.325	205.3047	205.3047	178.1348	220.6252	220.2635
Coars_SFM	8.029387	6.64764	6.64764	8.644174	6.497823	6.519396
Contrast_GLDM	117.8396	145.2067	145.2067	80.95061	111.3427	151.6841
Contrast_SFM	15.48359	17.09781	17.09781	12.76588	14.97674	17.47459
Energy_GLDM	0.100305	0.07558	0.07558	0.100406	0.088066	0.072945
Entropy	2.549053	3.129006	3.129006	2.975264	3.304167	3.170626
Entropy_GLDM	2.52516	2.836492	2.836492	2.540842	2.64843	2.849696
Homogeneity GLDM	0.1816	0.135984	0.135984	0.164404	0.132915	0.125444
Kurtosis	3.905143	4.253785	4.253785	3.250713	3.013949	3.537137
M	1.002388	1.00664	1.00664	1.00396	1.010146	1.006431
Mean	237.3125	183.322	183.322	182.5238	156.1905	181.4853
Mean_GLDM	8.224513	9.239634	9.239634	7.028659	8.385366	9.558537
Median	239.2813	185.9744	185.9744	184.0139	158.0286	184.0536
Period_SFM	0.518914	0.536565	0.536565	0.527658	0.627303	0.557147
Radial Sum	1666.889	3859.078	3859.078	3838.339	3294.79	3820.083
Roughness_SFM	2.551193	2.516996	2.516996	2.483829	2.419382	2.520933
Skewness	-1.06682	-1.00284	-1.00284	-0.59668	-0.53808	-0.72151
TEM1	13074.7	52920.75	52920.75	26675.87	35660.02	46723.36
TEM2	930.4136	1760.291	1760.291	1202.106	1412.693	1602.614
TEM3	184.8609	390.026	390.026	265.0212	253.4465	383.8651
TEM4	5265.371	8977.38	8977.38	6080.846	7709.646	8422.891
TEM5	443.8413	846.7284	846.7284	551.7337	584.4726	775.1799
TEM6	2868.084	3695.78	3695.78	2553.35	3123.902	3565.015

5.2 DIMENSIONALITY REDUCTION

As already discussed in the chapter 4, the abundance of features makes the data analysis more complex and hectic, hence need of dimensionality reduction. The features are reduced in such a way that, they yield maximum accuracy upon classification. In this work, 8 features are extracted from 26 initial features using FDR. The dimensionality is further reduced to 6 by using Sequential Backward Selection (SBS) method. Following are those 6 features

1) Homogeneity
2) M
3) Median
4) Entropy
5) Energy
6) Radial sum.

5.3 CLASSIFICATION

The following tables show the classification result for different combinations of texture features. Table 5.4.1 to 5.4.4 shows the classification accuracy for k-NN classifier for the k-values 1,3,5,7 respectively. As already discussed in the chapter 3, the value of *k* has large impact on the classification accuracy. For avoiding conflict odd k-values are taken in to consideration. The k-value that is showing best accuracy is finally chosen. It can be seen from the observation that k-value equal to three gives better accuracy.

Table 5.5 Table showing classification accuracy for the k-value one, for different feature combination.

	FRACTAL2	**M**	**Median**	**Entropy**	**Energy**	**Radial Sum**
FRACTAL2		57.14	74.72	46.15	49.45	75.52
M	57.14		86.81	84.61	84.61	84.61
Median	74.72	86.81		91.2	86.81	81.31
Entropy	46.15	84.61	91.2		53.84	84.61
Energy	49.45	84.61	86.81	53.84		80.21
Radial Sum	75.72	81.31	81.31	84.61	80.2	

Table 5.6 Table showing classification accuracy for the k-value three

Feature	**FRACTAL2**	**M**	**Median**	**Entropy**	**Energy**	**Fr**
FRACTAL2		59.31	71.42	46.15	42.85	71.82
M	59.31		87.91	84.61	74.72	82.41
Median	71.42	87.91		92.3	89.01	79.12
Entropy	46.15	84.61	92.3		53.84	84.61
Energy	42.85	74.72	89.01	53.84		84.61
Radial Sum	71.82	82.41	79.12	84.61	84.61	

Table 5.7 Table showing classification accuracy for the k-value five

	FRACTAL2	**M**	**Median**	**Entropy**	**Energy**	**Fr**
FRACTAL2		59.34	76.92	45.05	50.54	72.52
M	59.34		81.31	81.31	76.92	81.32
Median	76.92	81.31		89.01	86.81	75.82
Entropy	45.05	81.31	89.01		48.35	84.61
Energy	50.54	76.92	86.81	48.35		83.51
Radial Sum	75.52	81.32	75.82	84.61	83.51	

Table 5.8 Table showing classification accuracy for the k-value seven

Feature	**FRACTAL2**	**M**	**Median**	**Entropy**	**Energy**	**Fr**
FRACTAL2		58.24	74.72	41.75	50.54	72.52
M	58.24		75.82	79.12	71.42	81.31
Median	74.72	75.82		85.71	84.61	76.92
Entropy	41.75	79.12	85.71		39.56	82.41
Energy	50.54	71.42	84.61	39.56		83.51
Radial Sum	72.52	81.31	76.92	82.41	83.51	

Here, we can see that every time *k*-value is changed, the accuracy is changing. Finding *k*-value that gives best result is of prime importance. From these tables we can see that intitially when *k*=1, the accuracy is less. As *k*-value is increasing, the accuracy reached a pea*k* and then started decreasing for *k*=5 and 7. The maximum accuracy is found for *k*=3, and hence this value of *k* is used in further analysis.

Table 5.9. The table showing accuracy in percentage for various combinations of attributes for different classifiers.

	FRACTAL2, M	FRACTAL2, Median	FRACTAL2, Entropy	FRACTAL2, Energy	FRACTAL2, Radial Sum	M, Median	M, Entropy	M, Energy	M, Radial Sum	Median, Entropy	Median, Energy	Median, Radial Sum	Entropy, Energy	Entropy, Radial Sum	Energy, Radial Sum
k-NN	59.34	71.42	46.15	42.85	71.42	87.91	84.61	74.72	82.41	**92.3**	89.01	79.12	53.84	84.61	84.61
Random Forest	69.23	79.12	46.15	40.65	73.62	89.01	87.91	86.81	85.51	**92.3**	85.71	76.72	50.54	85.71	80.21
C 4.5	70.32	74.72	42.85	38.46	72.52	80.21	84.61	82.41	76.92	**87.91**	74.72	74.72	40.65	87.91	79.12
CART	68.13	82.41	34.06	38.46	78.02	82.41	86.81	85.71	80.21	**89.01**	87.91	82.41	45.05	85,71	84,61
Naïve Bayes	74.72	74.72	51.64	45.05	64.83	83.51	84.61	84.61	80.21	**82.41**	81.31	68.13	32.96	74.72	74.72
Average	68.348	76.478	44.17	41.094	72.082	84.61	83.73	82.85	80.65	**88.78**	83.73	76.24		83.73	80.67
Classifier Ensemble	71.42	81.31	46.15	41.75	79.12	86.81	87.91	84.61	82.41	**94.5**	93.4	79.12	49.45	91.2	90.1

The table shown above presents accuracy for various combinations of attributes for different classifiers. It can be seen that the feature combination of Median and Entropy, shown in shaded cells, gives best result for all the classifiers. The table also presents the average of accuracies of all the classifiers, and the result of classifier ensemble. The reason for being having better inter-class separation between Median and Entropy, they show very good results.

The classification results such as TP rate, FP rate, AUC etc for the feature combination Median and Entropy which has best result in terms of accuracy as shown in table 5.10

Table 5.10. Table showing TP rate,FP rate,AUC, precision values.

Class	TP Rate	FP Rate	Precision	Recall	F-Measure	AUC
Acute	0.897	0.032	0.929	0.897	0.912	0.973
Chronic	0.963	0	1	0.963	0.981	0.998
Haemorrhage	1	0	1	1	1	1
Normal	0.95	0.042	0.864	0.95	0.905	0.967
Weighted Average	0.945	0.02	0.947	0.945	0.946	0.983

5.4 CONFUSION MATRIX

Confusion matrix is another way of representing the classifier result. It gives numbers of correctly and falsely classifier instances out of the total instances. Higher the values of the diagonal and lower the values of the other elements, better is the result. The table 5.7 shows the confusion matrix resulted from classifier-ensemble. The diagonal elements are shown in shaded cells. It is seen from the table that, in some instances non-dioganal elements show very low or zero values – which is always expected from a good classifier.

Table 5.11 Confusion matrix.

Acute	Chronic	Haemorrhage	Normal	Classified as
26	0	0	3	Acute
1	26	0	0	Chronic
0	0	15	0	Haemorrhage
1	0	0	19	Normal

5.5 RECEIVER OPERATING CHARACTERISTICS (ROC)

ROC curve for a binary classifier is a curve plotted between True Positive (TP) and False Positive (FP) rates at different thresholds. This curve helps us to select optimum threshold. Area under the Curve (AUC) is the area covered by the ROC curve under it. The range of AUC is 0 to 1. Nearer the AUC to 1, better is the classifier performance. TP rate and FP rate are given by,

$$TPR = \frac{TP}{TP+FN}$$

$$FPR = \frac{FP}{TN+FP}$$

where, TN is True Negative instances, FP is False Positive instances, FN is false negative instances. Figures 5.1 to 5.3 shows ROC curves for the classes Acute, Hemorrhage, and Chronic respectively.

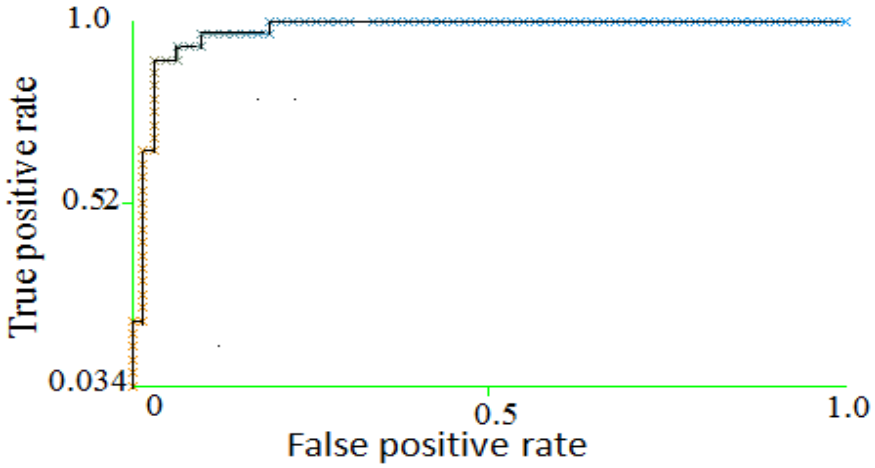

Fig 5.1 ROC curve for the class Acute. AUC= 0.973

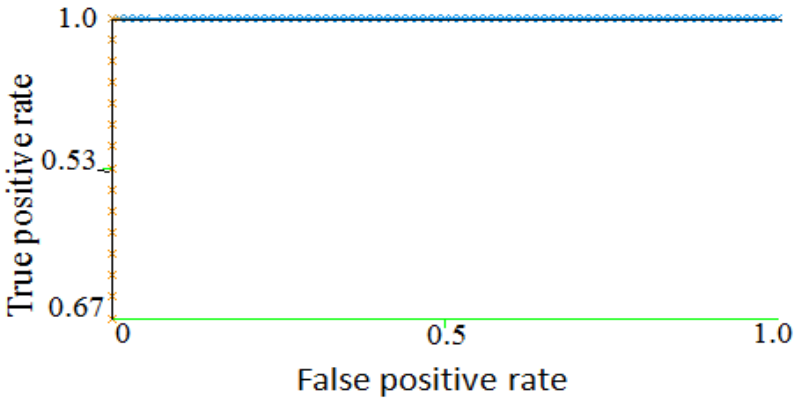

Fig 5.2 ROC curve for the class Hemorrhage. AUC= 1

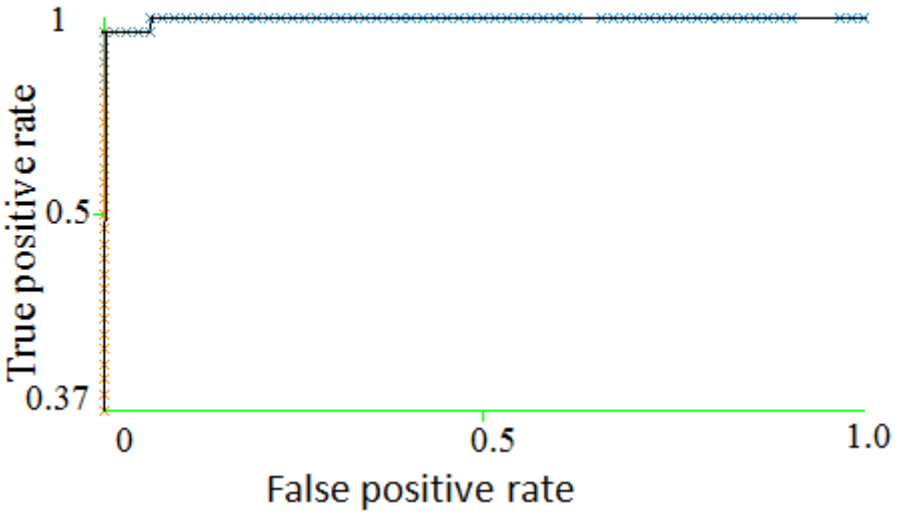

Fig 5.3 ROC curve for the class Chronic. AUC= 0.998

5.7 SCATTER PLOT

Scatter plots is a plot drawn between two features. It shows how feature elements are spread in the feature-space. More the concentration of the elements near the mean and higher the inter class distance; better is the feature-set for classification in terms of accuracy. The following figures plot between two features for the best feature-sets those we have got from the table 5.5. Figure 5.6 is the scatter plot between the features Median and Entropy, whose combination has given accuracy of 94.50%.

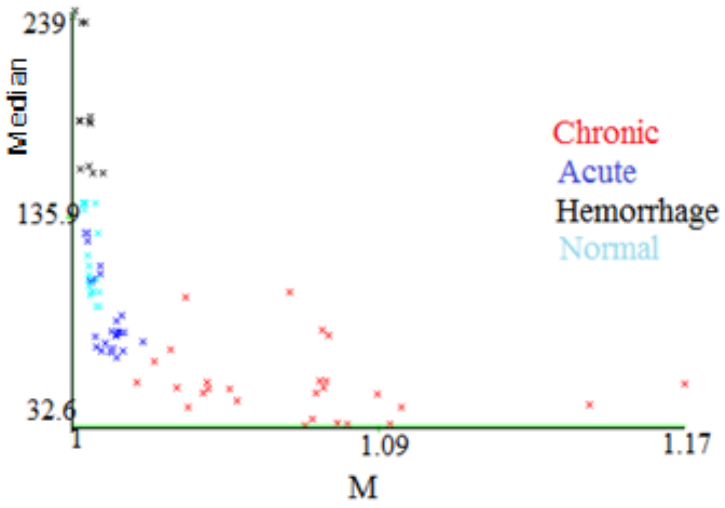

Fig 5.4 Figure showing scatter plot between the features M and Median

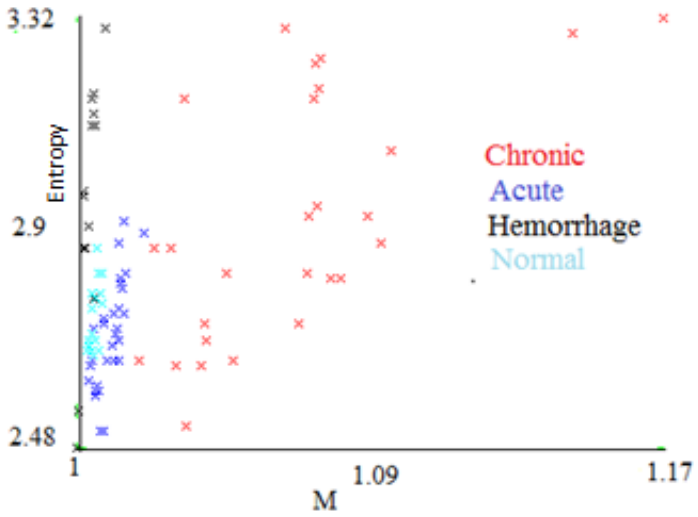

Fig 5.5 Figure showing scatter plot between the features Entropy and M

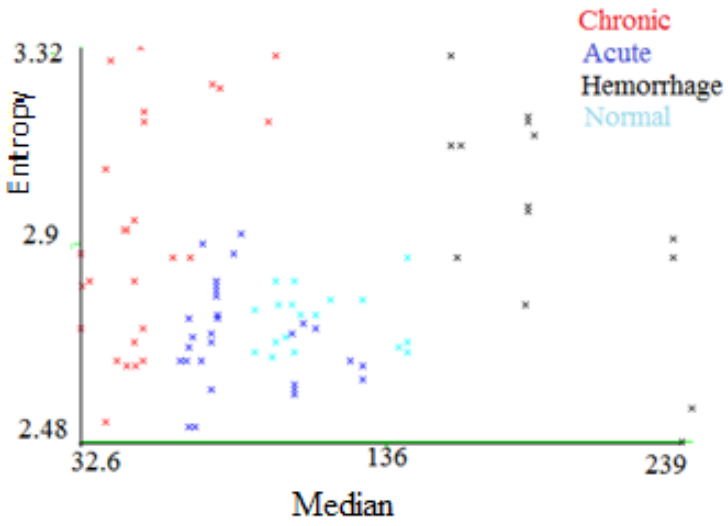

Fig 5.6 Figure showing scatter plot between the features Median and Entropy

CHAPTER-6
CONCLUSION AND FUTURE SCOPE

6.1 CONCLUSION

This thesis work presents classification of stroke using texture analysis. A part of the total work was done on MATLAB, Version 7.10. 26 texture features are extracted from 50 in-enhanced CT images, showing different stroke symptoms. In a total 91 instances were taken in to consideration for the analysis. Using Fisher's Discriminate Analysis (FDR), the initial dimension was reduced to 6 which were then used for statistical analysis using the software Weka , version 3.6. Some of the decisive points of the result are listed below.

- Classifiers used : k-NN, Bayesian, Random Forest, Decision Tree C 4.5,CART , and Support Vector Machine. Because poor result obtained from SVM classifier, it was not considered for final analysis.
- Out of six texture features used for final analysis, the feature combination of Median and Entropy was giving best result. The accuracy we could obtain from this feature combination was 94.5%. These features could give better result because of good inter-class separation, as shown in the scatter plot.
- AUC: Area under ROC was 0.945, 0.998, and 1 for Acute, Chronic and hemorrhage symptoms respectively. It tells that the algorithm used for detecting and classification of various types of is highly accurate and reliable, and can be implemented in real life applications.

It shows that texture features can be effectively used for classification of stroke. The classifiers used were best data mining algorithms; hence they are more reliable too. It also shows that normal un-enhanced CT images can be effectively used for correct diagnosis of stroke type in developing and underdeveloped countries which cannot afford costly MRI machines or any other techniques.

6.2 FUTURE SCOPE

Even though it is proved that texture analysis is a very effective tool for diagnosis of various types of stroke, because of very nature of the latter's, in some instances it is very difficult to differentiate between different types of stroke. Some of the future scopes are listed below.

- As already mentioned, the natures of the symptoms are very overlapping sometimes. Hence there is a need to develop a method that can elevate the presence of the symptoms which eventually help physicians to well differentiate the affected part of the brain and its nature.
- Artificial intelligence based diagnosis methods can be helpful to automatically detect the pert of the brain that is affected and to classify them. Particularly for Transient Ischemic Stroke, it is very much important as it shows very less or no presence of the problem.
- CT imaging is more patient friendly both in terms of time taken to scan and less hazardous when compared to MRI. Also the technology is easily available and affordable. Hence finding a newer way to diagnose stroke using new texture features which can help better differentiate the symptoms would be a great work.

REFERENCES

1. Fiona.C.Taylor : "Stroke in India." South Asia Network for Chronic Disease.2010

2. Dalal *et.al.* : "Population-Based Stroke Survey in Mumbai, India: Incidence and 28-Day Case Fatality." Neuroepidemiology. Vol 31, 2008.

3. Rosamond *et.al. :* "Heart Disease and Stroke Statistics—2007 Update." A Report From the American Heart Association Statistics Committee and Stroke Statistics Subcommittee,2007.

4. De Lucas EM, Sanchez E, Gutierrez A, et al.*"* CT protocol for acute stroke: tips and tricks for general radiologists". *Radiographics 2008;*

5. Mullins *et.al. :* "CT and Conventional and Diffusion-weighted MR Imaging in Acute Stroke: Study in 691 Patients at Presentation to the Emergency Department". *Radiology,* August 2002

6. Kunitz S, Gross C, Heyman A, et al. "The pilot stroke data bank: definition, design, and data". Stroke. 1984;15(4):740-746.

7. Jäger HR. "Diagnosis of stroke with advanced CT and MR imaging". Br Med Bull 200

8. A.D Lopez, C.D Mathers, Ezzati M, D.T Jamison, C.J Murray. "Global and regional burden of disease and risk factors", 2001: systematic analysis of population health data. *Lancet*. 2006;367:1747–1757.

9. Tamura, H., S. Mori, and Y. Yamawaki, "Textural Features Corresponding to Visual Perception," *IEEE Transactions on Systems, Man, and Cybernetics*, SMC-8, pp. 460-473, 1978.

10. Sklansky, J., "Image Segmentation and Feature Extraction," *IEEE Transactions on Systems, Man, and Cybernetics*, SMC-8, pp. 237-247, 1978.

11. Becker, B.; Drechsler, R.; , "Exact minimization of Kronecker expressions for symmetric functions ," *Circuits and Systems, 1996. ISCAS '96., Connecting the World., 1996 IEEE International Symposium on* , vol.4, no., pp.388-391 vol.4, 12-15 May 1996

12. W. H. Press, B. P. Flannery, S. A. Teukolsky, and W. T. Vetterling, Numerical Recipes, "The Art of Scientific Computing". Cambridge, U.K.: Cambridge Univ. Press, 1987.

13. K. I. Laws, "Rapid texture identification," Proc. SPIE, vol. 238, pp. 376–380, 1980.

14. J. S. Weszka, C. R. Dyer, and A. Rosenfield, “A comparative study of texture measures for terrain classification,” IEEE Trans. Syst., Man, Cybern., vol. SMC-6, Apr. 1976.

15. B. B. Mandelbrot, “The Fractal Geometry of Nature. San Francisco”, CA: Freeman, 1982.

16. C.M. Wu and Y.C. Chen, “Statistical feature matrix for texture analysis,” CVGIP: Graphical Models Image Processing, vol. 54, no. 5, pp. 407–419, September 1992.

17. Calvin C. Gotlieb, Herbert E. Kreyszig, “Texture descriptors based on co-occurrence matrices”, Computer Vision, Graphics, and Image Processing, Volume 51, Issue 1, July 199

18. R. A.Fisher,. (1940), “The Precision Of Discriminant Functions. Annals of Human Genetics”, 10: 422–429. doi: 10.1111/j.1469-1809.1940.tb02264.x

19. T.Cover.;P. Hart.; , "Nearest neighbor pattern classification," *Information Theory, IEEE Transactions on* , vol.13, no.1, pp.21-27, January 1967

20. Chih-Wei Hsu; Chih-Jen Lin; , "A comparison of methods for multiclass support vector machines," *Neural Networks, IEEE Transactions on* , vol.13, no.2, pp.415-425, Mar 2002

21. Tin Kam Ho; , "Random decision forests," *Document Analysis and Recognition, 1995., Proceedings of the Third International Conference on* , vol.1, no., pp.278-282 vol.1, 14-16 Aug 1995

22. A.M Prasad, L.R Iverson, A Liaw (2006) “Newer classification and regression tree techniques: bagging and random forests for ecological prediction”. Ecosystems 9(2):181–199

23. Tin Kam Ho;, "C4.5 decision forests," *Pattern Recognition, 1998. Proceedings. Fourteenth International Conference on* , vol.1, no., pp.545-549 vol.1, 16-20 Aug 1998.

24. L.I. Kuncheva, *Combining Pattern Classifiers: Methods and Algorithms*. Wiley-Interscience, 2004.